Fabrication and Characterization of a Hydrogel-Nanofiber Composite for Cartilage Replacement

by

Jacob Ludwick

May, 2020

Director of Thesis: Dr. Michelle Oyen

Major Department: Engineering

Articular cartilage plays a pivotal role in joint function, and when articular cartilage degrades, the function of the tissue declines. Osteoarthritis arises due to the declining health of articular cartilage and results in pain and swelling in the joint. Current treatments rely on using medication to mask the symptoms of osteoarthritis or replacing the joint with a prosthetic. These treatments fail to restore total function to the joint affected by osteoarthritis. By taking the principles of biomimicry and applying them to the knee, a cartilage substitute made from a poly(acrylic acid) and poly(vinyl alcohol) hydrogel is developed. Due to the brittle nature of hydrogels and the mechanical properties of load-bearing tissues such as cartilage, a reinforcement of electrospun gelatin nanofibers adds tensile strength to the matrix. Macro-scale indentation and mode III fracture are used to characterize the composite. By replicating the structure found in cartilage a more strong and tough composite material can be found to replicate the function of cartilage.

Fabrication and Characterization of a Hydrogel-Nanofiber Composite for Cartilage Replacement

EAST CAROLINA UNIVERSITY

A THESIS PRESENTED TO THE FACULTY OF THE DEPARTMENT OF ENGINEERING
IN PARTIAL FULFILLMENT OF THE REQUIREMENTS FOR THE DEGREE MASTER'S OF
SCIENCE IN BIOMEDICAL ENGINEERING

Jacob M Ludwick

May, 2020

Title:

By

APPROVED BY:
DIRECTOR OF
THESIS: _____
Name and Earned Degree

COMMITTEE MEMBER: _____
Name and Earned Degree

COMMITTEE MEMBER: _____
Name and Earned Degree

COMMITTEE MEMBER: _____
Name and Earned Degree

DEPARTMENT
CHAIRPERSON: _____
Name and Earned Degree

DEAN OF THE
GRADUATE SCHOOL: _____
Paul J. Gemperline, PhD

Contents

List of Tables

List of Figures

1 Introduction

1.1 Osteoarthritis and Cartilage

In the United States, osteoarthritis is the leading cause for disability affecting 53 million Americans. Contributing to 140 billion dollars in Medicare costs in 2013, and accounted for 164 billion dollars in lost wages due to the disability [2]. Cartilage is a type of connective tissue in the body that holds other tissues in place and also provides a protective covering for bones. Osteoarthritis is caused by the degradation of cartilage and, once destroyed, cartilage is unable to regenerate leading to pain and swelling in the joint.

There are three main types of cartilage; hyaline cartilage, elastic cartilage, and fibrocartilage. Each type can be found in different locations in the body and have slight variations in their composition to match their function. Cartilage has three main components, water, collagen, and proteoglycans. The types of collagen, the numerous proteoglycans, the ratios between the components, and the amount of water inside of the matrix determines the type of cartilage [3]. Regardless of function, all cartilage is avascular, meaning that nutrients are supplied to the tissue by diffusion from surrounding tissue due to the lack of a blood supply. All cartilage is also mainly composed of extracellular matrix with only a small percentage of cells to maintain the tissue. Both of these factors, the lack of a vascular network and the limited number of cells, contribute to cartilage's inability to regenerate after damage [4]. Articular cartilage, a type of hyaline cartilage named for the proteoglycan hyaluronin found in the tissue, is especially susceptible to damage due to the environment in which it is found. Articular cartilage is found at the ends of long bones and is subject to repeated loading and unloading in multiple planes. Articular cartilage must exhibit good shear properties due to the sliding motion seen during flexion of the knee and good compressive properties due to the loading during the heel strike phase of motion. Damage to articular cartilage can be the result of sport injuries such as an ACL tear, damage can also manifest as a result of wear due to age. Articular cartilage performs two main functions, it serves as a cushion to absorb loads and impacts and also provides a near friction-less surface for the joint to articulate. Damage to articular cartilage reduces the ability of the tissue to absorb the loads

Component	Wet weight
Water	68-85%
Collagen (type II)	10-20%
Total proteoglycans	5-10%
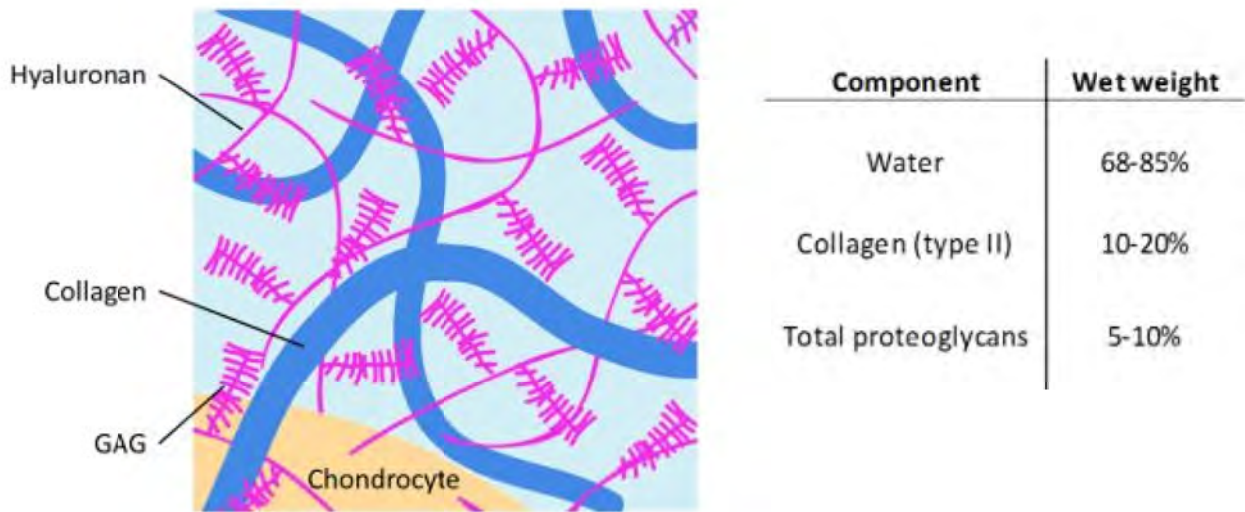
Figure 1.1: The structure of articular cartilage showing the proteoglycans and chondrocytes. Adapted From: [5].

found inside of the knee and also increases the amount of friction in the joint. This creates a positive feedback loop where the more damage there is to the tissue, the faster the tissue will decay.

Articular cartilage, a glossy and translucent material, is composed of 68-80% water, 10-20% type II collagen and 5-10% proteoglycans [3]. These three components are necessary in the proper proportions to maintain healthy and functional cartilage. The values of the components of cartilage change dependeing on the location that they are measured from. Measured close the the subchondral bone, the water content is about 68%. Measured from the surface, the water content reaches 80% [6]. Collagen fibers orient themselves in different directions depending on their depth in the articular cartilage. Near the surface of cartilage, the fibers are oriented parallel with the surface of the cartilage as this reduces the amount of friction and allows the collagen fibers to resist the shear forces produced by the flexion of the knee joint. [3, 7]. The collagen fibers closer to the subchondral bone are perpendicular to the surface of cartilage and act to anchor the tissue into the bone. Cartilage is able to withstand pressures of 10.1 MPa [6]. The stiffness of cartilage mainly comes from the inclusion of proteoglycans. Nearly 50% of the stiffness is dependent of these molecules [3, 7]. The

Figure 1.2: X-ray of knees afflicted with osteoarthritis. The gap between the femur and tibia is much smaller than someone with healthy cartilage. The bone has also started to flatten due to the constant wear from movement.

collagen fibers are critical for the strength of the material by containing the proteoglycans in a smaller area and causing the like charges on the ends of the proteoglycans to repel, resulting in a more rigid structure [3, 6].

In order to aleviate cartilage's inability to regenerate, there are multiple different methods to help reduce the amount of wear in the knee or reduce the amount of pain felt. Cost effective ways to reduce the pain include exercise and losing weight. Injections of hyaluronic acid can also reduce swelling and friction in the knee. There is a large range of surgical techniques to promote the healing of articular cartilage. A non-invasive technique is a microfracture technique that stimulates the growth of cartilage. This technique provides a short term, about five years, fix for lesions to the articular cartilage before the cartilage is back to its origonal state [8, 9]. There are also autologous chondrogenesis and osteochondral allogenic transplantation as possible treatments. These treatments survive about 10 years in the body before a revision is needed [10, 11]. This limits the treatment to those who are young enough and willing to undergo multiple surgeries. The chondral defect repairs only

fix a lesion smaller than 4 cm, and cannot be used on people who already suffer from severe forms of osteoarthritis where the cartilage tissue is non-existent.

Total knee replacement involving the removal of the knee joint from the body and inserting a prosthetic is one of the most common ways to treat osteoarthritis. By placing a prosthetic inside of the body, the bone on bone contact that causes the pain associated with osteoarthritis is removed. These implants last about 20 years due to problems with stress shielding [12]. Stress shielding occurs due to the large mismatch in the material properties between the stainless steel and titanium used in prosthetic knees and bone. This mismatch in the material properties causes the stresses of walking to be funneled into the prosthetic, causing bone density loss. Stress shielding also means that once an implant is used, the person does not have enough bone mass to facilitate a secondary implant once the primary implant's life has ended.

The focus of this project is on the stiffness and toughness of a cartilage-like material rather than the surface friction because if the material cannot withstand the loads and forces seen during normal use, the implant will fail long before the implant fails due to the loss of material from frictional wear.

1.2 Using Engineering Materials to Mimic Cartilage

To replicate the three main components of cartilage; water, collagen, and proteoglycans, there are analogous engineering material that can be used. Hydrogels are able to hold large amounts of water, electrospun fibers can be used to replicate the collagen fibers, and charged ions can be introduced to mimic the use of proteoglycans.

1.2.1 Hydrogels

Hydrogels are a long chain polymer that can form bonds in a process called crosslinking that traps water inside of pores created by that process. This crosslinking allows the material to have a high volume of water in the substance, thus creating good compatibility with the sur-

rounding tissue [13]. Hydrogels come in many different varieties of material and mechanical properties which can be customized to meet the desired application. Hydrogels are commonly used as scaffolds on which cells are grown and differentiated. Poly (ethylene Glycol) (PEG) hydrogels are common due to their simplicity and their biocompatability [14, 15].

This ability to hold large volumes of water inside of the structure also limits how strong hydrogels can be. This water inside of the pores exerts an osmotic pressure on the polymer chains inside of the hydrogel causing many hydrogels to be brittle. To try and remedy this issue, hydrogels have been combined with a number of materials to increase their mechanical properties. Electrospun fibers and charged particles have both been used to increase the stiffness and strength of hydrgogels but still fall short of the values found in native tissue [16].

1.2.2   Electrospun Fibers

After introducing the hydrogel, the next material to be inserted into the composite is gelatin nanofiber mats. These fibers are generated from electrospinning, an inexpensive and effective way to produce micro-scale and nano-scale fibers. This low cost and ease of manufacture has led to their popularity in research [1, 16–19]. These fibers can be made from many different materials, polycaprolactone, gelatin, and other polymers. Combinations of polymers can also be used in electrospinnning. Combinations of polymers are commonly used when one polymer does not have a viable solvent. By introducing a second polymer that has an available solvent the first polymer can be electrospun. Gelatin has emerged as a popular choice as a material due to gelatin's availability, composition, and biocompatibility [18, 20–22]. This safety for human consumption is not found in other materials such as polycaprolactone. Gelatin historically has been used as a food additive to create gelatinous foods. Porcine cartilage is often used in the production of gelatin, which contains collagen in the tissue. This collagen comes in a form that is biocompatible, due to its acellular nature, and easy to use as a substitute for human collagen.

Many of the tissues used in the production of gelatin have a high percentage of collagen in them. The other factor that makes gelatin biocompatible is its solvent. Polycaprolactone

as a polymer is biocompatible, but the solvent used to put the polymer in solution of electrospinning, dimethylformamide and tetrohydrofuan are toxic to the human body [1]. One solvent for gelatin is acetic acid (vinegar) [23]. This solvent is a weak acid that is similar in nature to the lactic acid that is produced in the body during anaerobic respiration. The kitchen form of acetic acid, vinegar, is used in many different foods and sauces. This familiarity in foods and its similar structure to lactic acid found in the body, allows acetic acid to be broken down by the human body leading to its safety as a biocompatible solvent. This also reduces the amount of processing required to render the scaffolds safe as they are considered biocompatible after drying.

Electrospun fibers have also been implemented into hydrogels and tested to determine their fracture properties and failure behavior were examined [1,20]. The gels tested in these studies layered the fibers in different directions. Despite the fibers being on a much smaller size scale than the gels, the fibers caused a change in the mechanical behavior of the gels.

1.2.3 Addition of Charged Ions

Due to the importance of charged particles inside of cartilage [3, 6, 7], it is necessary to include charges into the artificial cartilage. This is achieved by the use of a cryo-gel [5]. These gels are made from a poly (vinyl alcohol), (PVA), and poly (acrylic acid), (PAA), base and repeatedly cycled using freeze thaw cycles to crosslink the gel physically. The gels are not activated until the addition of sodium hydroxide allows the hydroxide groups to attach to the PAA and make the chains negatively charged. The purpose of these gels is to take advantage of the fact that like charges repel each other and allow for a material to increase its compressive stiffness.

1.3 Proposed Solution

1.3.1 The Proposed Composite

In order to fulfill the requirements of a material that is safe to implant into the body and provide a material that is sufficiently robust, a composite composed of a hydrogel made from

poly(vinyl alcohol), (PVA), and poly(acrylic acid), (PAA), the addition of charged ions, and with a fibrous network of electrospun gelatin fibers has been fabricated and characterized. These three components together help mimic a specific part of articular cartilage. The hydrogel with 15% wt. polymer contains 85% wt. water, similar to the 68-80% water and the 10-20% collagen found in articular cartilage [3]. These values do not take into account the electrospun fibers added into the composite, contributing to the dry weight of the overall material. The challenge and focus of this project is to essentially build reinforced
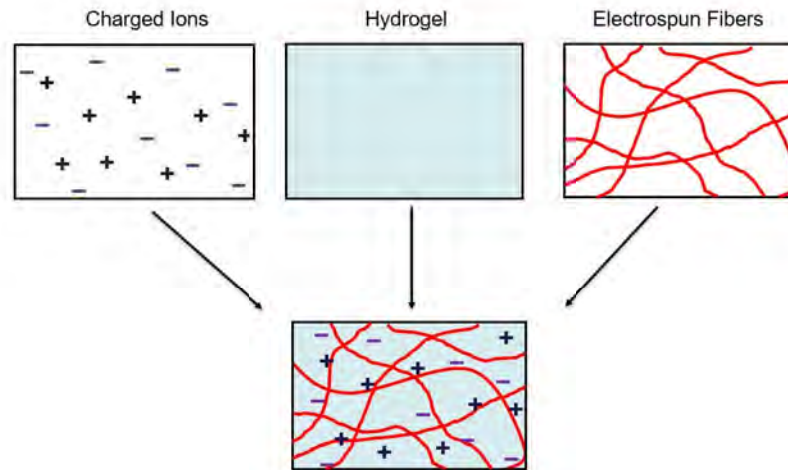
Figure 1.3: Diagram showing the three main components used in the proposed solution.

concrete on a micro-scale using materials that are safe for the body. The hydrogel can be analogous to concrete due to similar material behavior. Concrete, like hydrogels, performs better mechanically in compression than in tension. Despite this, concrete is used in the construction of bridges and buildings where it is placed in a bending scenario. In bending, a
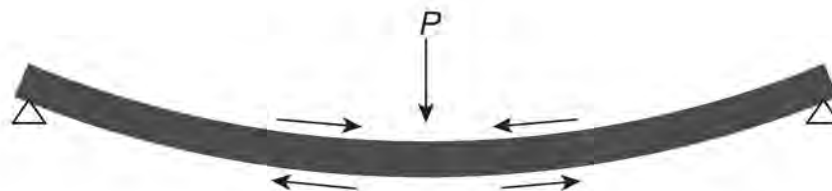
Figure 1.4: Diagram of a typical three-point bend scenario.

force, P, acts in the middle of the beam. This force causes the top of the material to be in compression due to the contraction of the material at the top surface and placed in tension

7

at the bottom surface due to the stretching of the material. To solve this, engineers place pre-tensioned steel beams inside of the concrete to keep the concrete in compression. In the proposed solution, the gelatin fibers act like the pre-tensioned steel beams keeping the hydrogel in compression. To accomplish this pre-tensioning of the electrospun fibers in the solution, the charged ions from the PAA interact to give a similar effect on the electrospun fibers.

1.3.2 Proposed Testing

For a biological material there are three important behaviors that must be taken into account. These mechanical behaviors are anisotropy, non-linearity, and time dependence. By choosing to analyze the materials using poroelastic and viscoelastic analysis, the time dependence of the materials is expected to contribute the largest portion the the material properties. By choosing to perform indentation testing, significant non-linear responses can be avoided, reducing the amount of error and increasing confidence in the values obtained. Anisotropy are changes to the material behavior based on the loading direction. This can be accounted for by performing testing in multiple axis to analyze the behavior in multiple directions. For this work, cartilage needs to be the most stiff in compression, but also resist tension as well. By isolating the effects of the three main effects time-dependence, non-linearity, and anistropy, a more complete picture of the material's mechanical behavior can be developed.

Indentation testing is important, because such testing allow us to determine the mechanical properties in a non-destructive way, which reduces the total number of gels that need to be fabricated. The indentation test also works well with gels due to their uneven surface. Compression tests require the strain of the material be tracked over time and an uneven or angled surface reduces the accuracy of those measurements. These experiments will be performed in distilled water rather than the synovial fluid, or an analog saline solution. In poroelastic analysis, the permability of the material is measured. Permability is a structural property of the material that is related to the time-dependent response of the material. The viscosity of the fluid does not have any impact on the assesment of this structural property [24].

The first test to characterize the gel are the viscoelastic tests. These tests will help determine the elastic modulus of the material and also give an upper bound for the modulus to help corroborate the value found in the poroelastic modulus. The poroelastic tests will determine the shear modulus of the material, which can be traced back to the elastic modulus, Poisson's ratio for the material, and the permeability of the material. By using small strains, any non-linear effects on the material will be small in comparison to the effects due to the time dependence of the material. Before performing the analysis, understand how viscoelasticity and poroelasticity relate, the equations and theory that govern the models and behavior of the materials discussed in this thesis must be explored. First by understanding the basic models of elasticity and how making more complex models allows a more thorough understanding of the material.

2 Mechanical Theory

2.1 Material Models

2.1.1 Elasticity

The most basic material model is the linear elastic model. This model comes from the assumption that linear elastic materials behave like a Hookean spring.

$$F = -kx \tag{1}$$

where F is the force applied to the spring, k is the spring constant in N/s, and x is the distance the distance from equilibrium. Elasticity uses this model as the basis for linear elastic materials. Firstly, the relationship between force and stress must be found first as the spring constant k is not a material constant and changes based on the cross-sectional area. The stress, σ is directly proportional to the applied force, P and cross-sectional area of the material.

$$\sigma = \frac{P}{A_0} \tag{2}$$

Any elastic material that experiences a load, experiences a change in length. The ratio between the initial unloaded length and the final loaded length is denoted as the strain of the material.

$$\epsilon = \frac{\Delta L + L_0}{L_0} \tag{3}$$

A material that behaves linearly, the stress inside of the material is also related to the strain of the material by the constant E, or the elastic modulus of the material

$$\sigma = E\epsilon \tag{4}$$

when a material is deformed the overall volume must stay the same as no material has been added or taken away. To accommodate for this, materials will either contract or expand in the lateral direction in response to a force. This ratio between the lateral change in length

is Poisson's Ratio ν

$$\nu = -\frac{\epsilon_{22}}{\epsilon_{11}} \tag{5}$$

ϵ_{11} is the strain in the loading direction and ϵ_{22} is the strain in the direction perpendicular to the loading direction. For isotropic linear elastic materials, Poisson's ratio is usually bounded between -1 and 0.5. Values outside of this range indicate significant effects from anisotropy.

For many engineering materials the elastic constants E and ν are enough to define a material fully. However, this assumes that the material is elastic and behaves linearly. For many biological materials this is not the case. Not only are biological materials inelastic, but many exhibit time dependent properties that change the stress inside of the material over time, anisotropy where the material exhibits different properties based on the axis of loading, nonlinear material behaviors. All of these material behaviors complicate the analysis and characterization of biological and biological-like materials.

2.1.2 Viscoelasticity

Linear elasticity is useful for materials that follow the simple stress-strain relationship. Most biological materials, however, do not behave in a linear elastic manner. Most biological materials exhibit time-dependent properties that are best explained by viscoelasticity. Viscoelaticisty, is comprised of components that can be represented by both elastic and viscous components. The elastic component can be described by a Hookean solid as shown above, the viscous component by a Newtonian fluid with viscosity η, deformation over time $\dot{\epsilon}$, and stress σ

$$\sigma = \eta \dot{\epsilon} \tag{6}$$

The simplest viscoelastic model places these two components in series as shown in Figure(2.1). This simple model allows the extraction of a simple expression that can be used to model time dependent behavior of materials based on two constitutive equations. Because each of the components are placed in series, the stress in the total system is the same as the
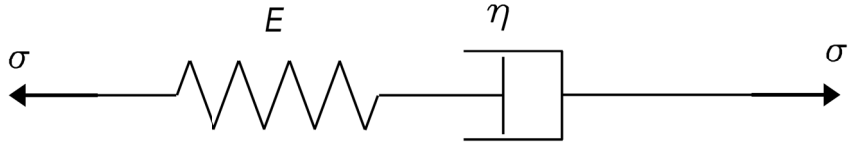
Figure 2.1: The Maxwell model for viscoelasticity.

stress in the individual components

$$\sigma_T = \sigma_s = \sigma_d \tag{7}$$

where σ_T is total stress, σ_s is the stress in the spring, and σ_d is the stress in the dashpot

$$\epsilon_T = \epsilon_s + \epsilon_d \tag{8}$$

where ϵ_T is the total strain, ϵ_s is the strain in the spring, and ϵ_d is the strain in the dashpot. By using these equations with the definitions for a Hookean spring and Newtonian fluid, the equation for the complete model is shown below

$$\dot{\epsilon} = \frac{\dot{\sigma}}{E} + \frac{\sigma}{\eta} \tag{9}$$

there are two characteristic responses for viscoelastic materials, creep and relaxation. Relaxation is the response to an instantaneous strain where the stress inside the material decreases over time. Creep, is the stress analouge of relaxation, where an instantaneous stress causes an increase in the strain over time. For the Maxwell model, only relaxation is observed due to the linear relationship between strain and time. For a model to exhibit both behaviors additional elements are needed which complicates the equations but increases the accuracy of the model. Therefore, a trade off must be made between the accuracy of the model and the simplicity of the calculations when conducting viscoelastic analysis [1].
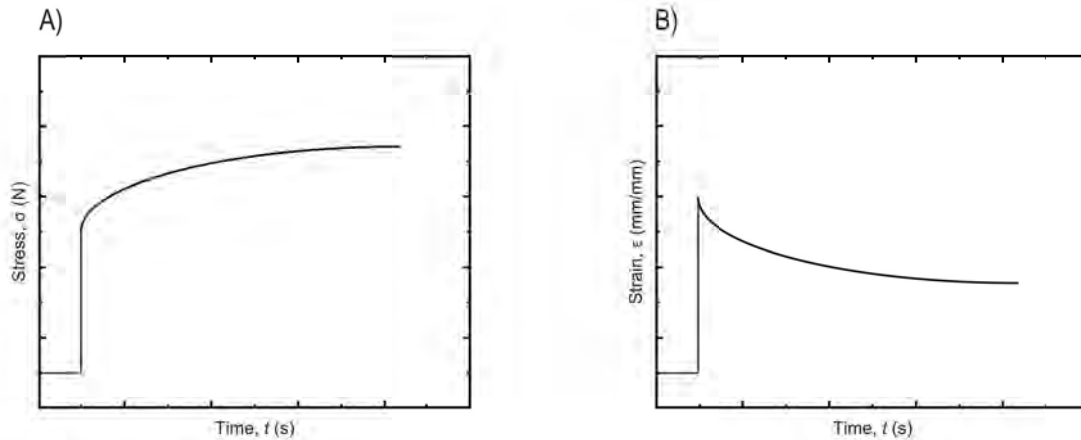
Figure 2.2: (A) the ideal response of a non-Maxwell viscoelastic material that experiences an instantaneous strain. (B) The ideal response of a non-Maxwell viscoelastic material that experiences an instantaneous stress.

2.1.3 Poroelasticity

Unlike the viscoelastic model, which allows analysis based on the material behavior and time-dependent response, the poroelastic model makes an assumption about the material structure and how the fluid and solid phase interact. Because the solid phase is also assumed to be incompressible, $\nu = 0.5$, the governing equations rely on analyzing the fluid movement through the pores of the gel during testing and the ratio between the undrained state where water is present in the solid and undrained where all the water has left the solid.
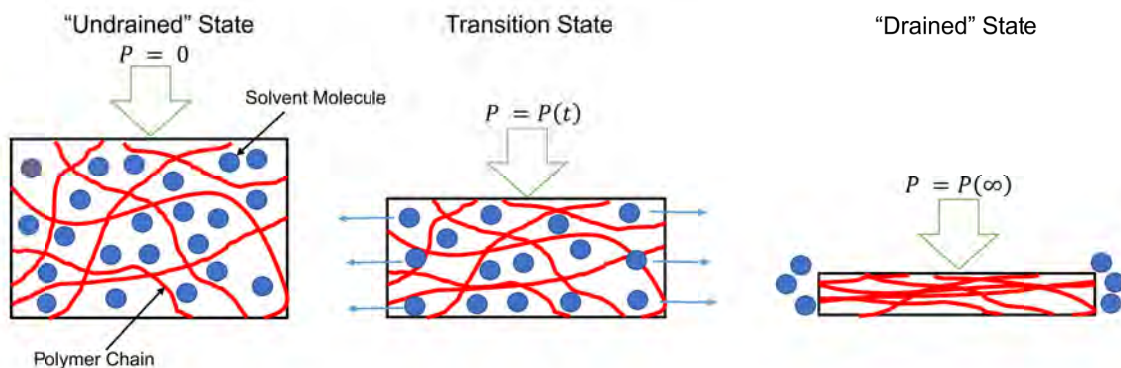
Figure 2.3: Three stages of a poroelastic material under loading. The undrained and unloaded state, the transition state, and the drained or equilibrium state.

Darcy's Law governs the movement of fluid through a solid with a pressure gradient and is

typically associated with movement of water through rocks in geological analysis where the incompressible assumption is valid

$$q_i = -\kappa \frac{dp}{dx_i} \tag{10}$$

where q_i is the fluid flux through the solid and κ is the permeability of the material. The benefit to using poroelasticity over viscoelasticity is the assumption of the material structure that comes when using a poroelastic model.

2.2 Mechanical Testing

Testing a material intended to replace cartilage requires multiple tests to determine the properties of that material due to the multiphasic nature of cartilage. Cartilage is classified as a biphasic material meaning that its properties cannot be described by a singular property such as Young's modulus. Because of the complex behavior of the material, multiple tests are needed to determine the mechanical properties. This project will use two mechanical tests, an indentation test and tensile test. Indentation is the process by which a small probe is pushed into the surface of a material and determine the force required to create a small size indentation. Another important value that is found during indentation is the strain relaxation time. This is the time it takes for a material to return to normal after the applied force is removed. In a biphasic material, this is important to determine the stiffness of the material [1]. The downsides of this test are that it does not address the aniostropy found in cartilage like materials and indentation below strains of 10% do not introduce non-linearities into the data.

Changes in the surface morphology over the material can lead to different results in the stiffness of the material. To remedy this, multiple tests are needed over the surface and then averaged to generate a rough estimate for the stiffness of the material [5]. Tensile testing is used to determine the fracture toughness of the material. It has been found that the fibers used in cartilage like structures show ductile behavior away from the brittle behavior of pure hydrogels [16]. This tensile test is designed to be paired with the indentation test to fully characterize a material.

2.3 Volume Swelling

The swelling ratio of a hydrogel can be found by measuring the dry weight of the hydrogel and comparing it to the swollen hydrogel weight.

$$SwellingRatio = \frac{(W_s - W_d)}{W_d} \tag{11}$$

The polymer percentage in a hydrogel can be calculated by finding the percentage of water in the structure and subtracting from 100.

$$Polymer\,(\%) = \frac{W_d}{(W_d + W_s)} \times 100\% \tag{12}$$

The polymer percentage is related to the pore size of the structure. The higher the polymer content the smaller the pore size. This can also be related to the toughness of the material, because larger pore sizes lead to a more brittle hydrogel structure.

2.4 Fracture Toughness

To gather information on the behavior of the material a notch is placed to create a stress-concentration by decreasing the area of the material at the notch. This ensures that the critical area is in the same location each time, reducing the effects of small imperfections in the material. This notch is also what defines a test as a fracture test. Similar tests could be performed on 'pristine' un-notched samples but would be unable to calculate the toughness. Toughness is defined as the amount of energy needed to propagate a crack in the material, often confused with strength which is the stress at which a material fails, due to the similarity of the two modes of testing. Because biological materials exhibit high levels of compliance and experience large strains during testing, it is necessary to reduce the amount of deformation in the material. By using a mode III ('trouser tear') test, most of the energy goes to propagating the crack and not deforming the material. This test places the 'legs' of the sample perpendicular to the body and pulls on the sample like a pair of pant legs pulled in opposite directions, one leg forwards and one leg backwards. This places the material in pure shear loading which allows for the calculation of the fracture toughness of a material.
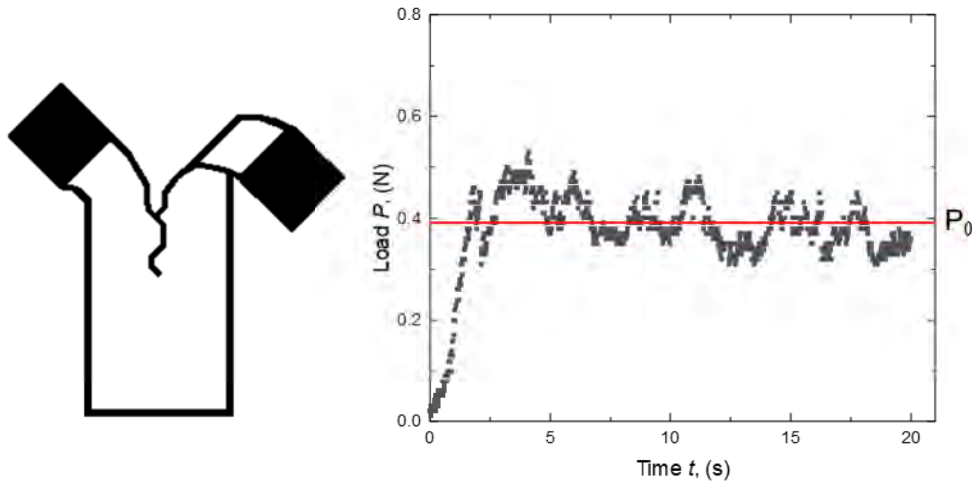
Figure 2.4: The left is an example of a sample that has undergone mode III shear testing. On the right is an example of how the average force is calculated for mode III shear.

The fracture toughness of a material is dependent on two parameters, the force of fracture denoted P_0, and the thickness of the material being tested t. These two are used in Equation 13 to determine the fracture toughness of the material.

$$T_c = \frac{2P_0}{t} \tag{13}$$

Only the thickness is needed here, because it is assumed that the total deformation of the sample is also the total length that the crack propagates, negating the need for an area in the equation. Fracture testing allows for the measurement of the toughness of the material, to determine the stiffness other forms of testing are needed.

2.5   Indentation Testing

Indentation testing is a form of mechanical testing that uses an indenter of a known geometry, a cone, sphere, or pyramid to determine the stiffness of a material. By using contact mechanics between a sphere and a flat plane, Hertzian contact mechanics, allows for the characterization of an unknown material.

2.5.1 Hertzian Contact

Hertzian contact is most commonly used for the evaluation of the stresses present in gears where two spheres are in contact. This can be used for an indentation test by changing the geometry to the contact between a shpere and a flat plane. To use Hertzian contact, the strains are assumed to be small; this allows elastic plastic materials to remain in the elastic region and prevents materials from deforming due to yielding. The continuous surface of the material simplifies the calculation of the area of contact, and the contact area is less than the radius of the indentation sphere. The contact is frictionless, so no energy is lost due to friction and all the force is directed into the material. There is also no adhesion between the two surfaces as this could result in a tensile force masking the true compressive force present in the material [19].

The variables critical to Hertzian contact include the material stiffness, reported as Young's modulus E, Poisson's ratio ν, the radius of the indenter probe R, the indentation depth h, the radius of the contact area between the two surfaces a, and the force needed to hold the indentation depth P. The indentation depth can also be determined by the force, the
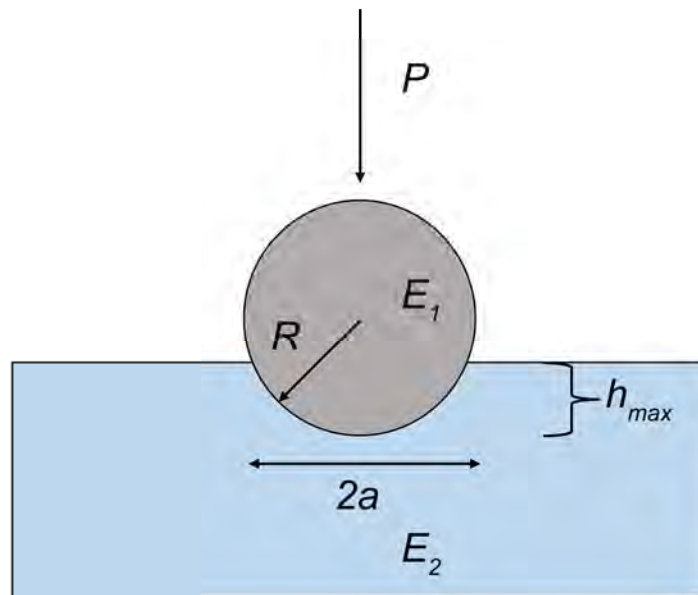
Figure 2.5: A typical indentation test and its parameters. (author's own)

relationship between the material stiffness and the radius if the indenter. The modulus of

the system is the strain present in the plane of indentation referred to as the plane strain elastic modulus.

$$\frac{1}{E_*} = \left(\frac{1 - \nu_1^2}{E_1} + \frac{1 - \nu_1^2}{E_2} \right) \tag{14}$$

The expected strain, ϵ, for the indentation can be found by relating the indentation depth, h, with the radius of the indenter probe, R.

$$\epsilon = 0.2 \left(\frac{\sqrt{h}}{\sqrt{R}} \right) \tag{15}$$

By assuming the Poisson's ratio of the gel is about 0.5, we can equate the plane strain modulus with the elastic modulus of the gel.

$$\frac{E}{1 - \nu^2} = \frac{4E}{3} \tag{16}$$

These two equations allow us to simplify and treat the elastic modulus of the gel as the only unknown if stiffness of the indenter probe is much greater than the gel. Steel has an elastic modulus of 200 GPa and is much stiffer than any gel or biological material we could test, so this assumption is valid.

This simplified equation allows the axial force in the system to be a function of the elastic modulus of the gel, the indenter probe radius and the indentation depth.

$$P = \frac{16\sqrt{R}}{9} h_0^{3/2} E \tag{17}$$

2.5.2 Viscoelastic Analysis

The Hertzian contact mechanics in indentation testing can be modified to include the time component necessary for viscoelastic analysis. In viscoelastic analysis the stiffness of the material changes as a function of time. A solution can be found by using the indentation load data and curve fitting the material response to the proper equation given a few initial guesses. However, because the material is assumed to be a viscoelastic material the shear modulus is used instead of the elastic modulus. The two can be related by the equation

below by assuming that the material is incompressible and Poisson's ratio is equal to 0.5.

$$G = E/3 \tag{18}$$

However, if Poisson's ratio is assumed to be another value the shear modulus can be found by relating the elastic modulus and the incompressible modulus ($\nu = 0.5$).

$$G = 2G^I(1-\nu) \tag{19}$$

By applying the Boltzmann hereditary integral to the equation above, the shear modulus as a function of time can be found [25]

$$P(t) = \frac{8\sqrt{R}}{3}h_0^{3/2}\left[G(t)\right] \tag{20}$$

However, because the shear modulus as a function of time is not known for the material and that there is no analytic solution to the equation, the shear modulus can be expressed as a two term Prony series. This substitution presents,

$$P(t) = \frac{8\sqrt{R}}{3}h_0^{3/2}\left[C_0 + \sum_{k=1}^{2} RCF_k C_k exp(-t/\tau_k)\right] \tag{21}$$

To fit the equation to the data, preliminary guesses for the coefficients are needed. The initial guess of C_0 will be found by solving equation two at $t = \infty$ with load at the end of the time period $P(t)$. The time constant guesses will be the rise time and hold time for the experiment allowing for the substitution of those same coefficients in the elastic modulus equation.

$$E(t) = C_0 + \sum_{k=1}^{2} C_k exp(-t/\tau_k) \tag{22}$$

2.5.3 Poroelastic Analysis

Poroelastic analysis is used to derive three important material constants, Poisson's Ratio ν, the permeability of the material κ, and the shear modulus of the material G. Hu et al (2011), used indentation to find these constants for gels by starting with a modified form of

Darcy's law

$$Q_i = -\left(\frac{k}{\eta \Omega^2}\right)\frac{\partial \mu}{\partial x_i} \tag{23}$$

where κ is the permeability, Ω is the volume per solvent molecule, μ is the chemical potential of the gel, and η is the viscosity of the solvent. Because Ω and η are constants for well known gel solvents, e.g. water, the equation simplifies to the diffusion equation

$$\frac{\partial C}{\partial t} = D\nabla^2 C \tag{24}$$

where D is the diffusivity of the material where C is the concentration of the solvent in the gel

$$D = \frac{2(1-\nu)}{(1-2\nu)}\frac{G\kappa}{\eta} \tag{25}$$

this equation normally is unable to be solved analytically, but for indentation, the instant the indenter probe makes contact with the surface of the gel there is not time for the solvent to move out of the gel and $C = C_0$. The gel at this instant acts like an incompressible solid so $P(0) \propto G$. The initial force is calculated differently for different geometries. For spherical indentation

$$P(0) = \frac{16G}{3}ha \tag{26}$$

where a is the contact area of the indenter probe and for spherical indentation

$$a = \sqrt{rh} \tag{27}$$

at the end of the indentation test, the fluid has reached equilibrium such that the material behaves like a compressible elastic solid

$$P(\infty) \propto \frac{G}{2(1-\nu)} \tag{28}$$

and due to the relationship between $P(0)$ and G, ν is easily calculated as the ratio of the initial force and the equilibrium force

$$\frac{P(0)}{P(\infty)} = 2(1 - \nu) \tag{29}$$

the last material constant that needs to be found is κ. During the transition from the instantaneous force and the equilibrium force, the solvent moves through the material over the contact area. At any time t, the solvent has moved a distance of $\sqrt{Dt}$. The function can be written as

$$\frac{P(t) - P(\infty)}{P(0) - P(\infty)} = g(\tau) \tag{30}$$

τ is the normalized time for the function $g(\tau)$ and is specific to the geometry of the indenter being used.

$$\tau = \frac{Dt}{a^2} \tag{31}$$

By using a curve fitting algorithm the data from the indentation test can be fit to the function $g(\tau)$ and the diffusivity of the material can be found.

2.6 Conclusions

There are two types of testing being conducted that require different separate analysis. The simplest analysis being the mode III shear analysis. This calculates the fracture toughness of the material by averaging the force over the duration of the fracture test over the thickness of the material. For indentation, there are two different analysis with their strengths and weaknesses. There is the viscoelastic analysis that models the material time dependent behavior. The analysis requires a curve-fitting algorithm to fit the data generated from the test to the equation in the analysis. Poroelastic analysis acts similar to the viscoelastic analysis, requiring a curve-fitting algorithm to conduct the analysis. The main difference between the viscoelastic and poroelastic analysis is the assumption about the structure of the material being tested. When using poroelastic analysis there is an assumption that the material has a porous structure. Next, preliminary experiments conducted on the volume swelling of hydrogels, the time-dependent analysis of simple single-polymer hydrogels, and

21

the fracture testing of paper are discussed to develop procedures for the testing of the composite materials.

3 Preliminary Tests

3.1 Volume Swelling

3.1.1 Introduction

Hydrogels have been investigated for their use in biomimetic materials because of their ability to hold large volumes of water. Sodium poly (acrylate) is a polymer that absorbs large amounts water to create hydrogels and has seen extensive commercial use in infant diapers and artificial snow. The volume swelling of a hydrogel is the ratio between the weight of the dry polymer compared to the weight of the hydrogel at equilibrium. This allows for the calculation of the amount of water inside of the hydrogel structure. The swelling of a
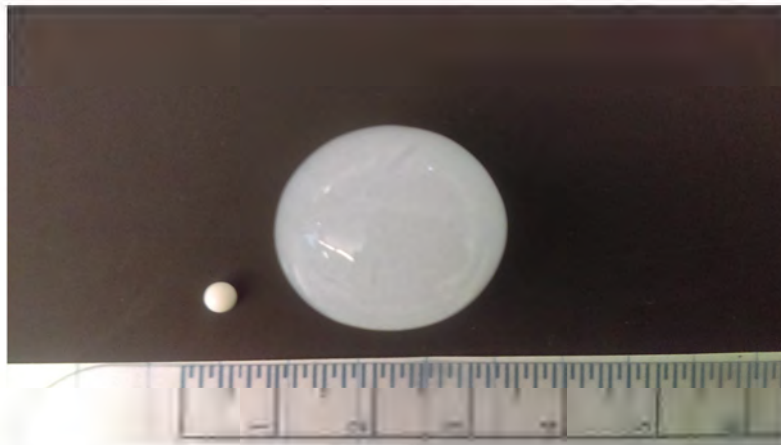
Figure 3.1: A dehydrated hydrogel bead that is only a few millimeters in diameter next to a similar hydrogel bead in its equilibrium state, scale is in cm. (author's own)

hydrogel can be calculated by tracking its change in mass and size over time. The ratio of the dry and swollen volume and mass of a hydrogel are correlated to the mechanical properties that the hydrogel exhibits. Hydrogels with a higher percentage of water behave more brittle, while hydrogels with a lower percentage of water are more ductile. In water the sodium ions fall off the sodium poly (acrylate) structure and water is absorbed as the polymer chains form pockets around the water. These pockets swell and is where the water in the hydrogel is stored.
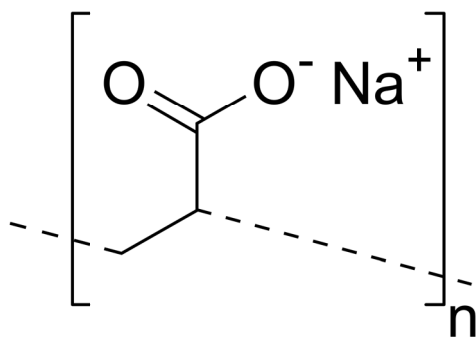
Figure 3.2: The chemical structure of sodium poly (acrylate). Taken From: https://commons.wikimedia.org/wiki/File:Sodium_polyacrylate_skeletal.png Date Accessed: 4/17/19

3.1.2 Methods

Twelve super absorbent polymer spheres (Carolina Biological Supply Company, Burlington, NC) were weighed and placed into beakers filled with 25 ml of water. At 30, 60, 90, 120, 180, 240, 300, 1460, and 5760 minutes, the individual beads were weighted and a picture of the beads was taken next to a ruler (e.g. Figure 3.3). This picture was then imported into

Figure 3.3: A super absorbent polymer bead imported into ImageJ with the line draw that measures the diameter.

ImageJ and the diameter of the bead measured with relation to a the centimeter scale placed next to the bead. This process was repeated until the beads reached equilibrium after four days.

24

3.1.3 Results

The average swelling ratio between the twelve beads was 2500 times. The equation takes the weight of the dry polymer bead, W_d, and the weight of the swollen hydrogel, W_s, to calculate the ratio using Equation 11. The weight of the hydrogel beads increased as time went on until equilibrium was reached. The volume of the hydrogel beads increased exponentially as time passed. The polymer percent was calculated by comparing the dry weight of the
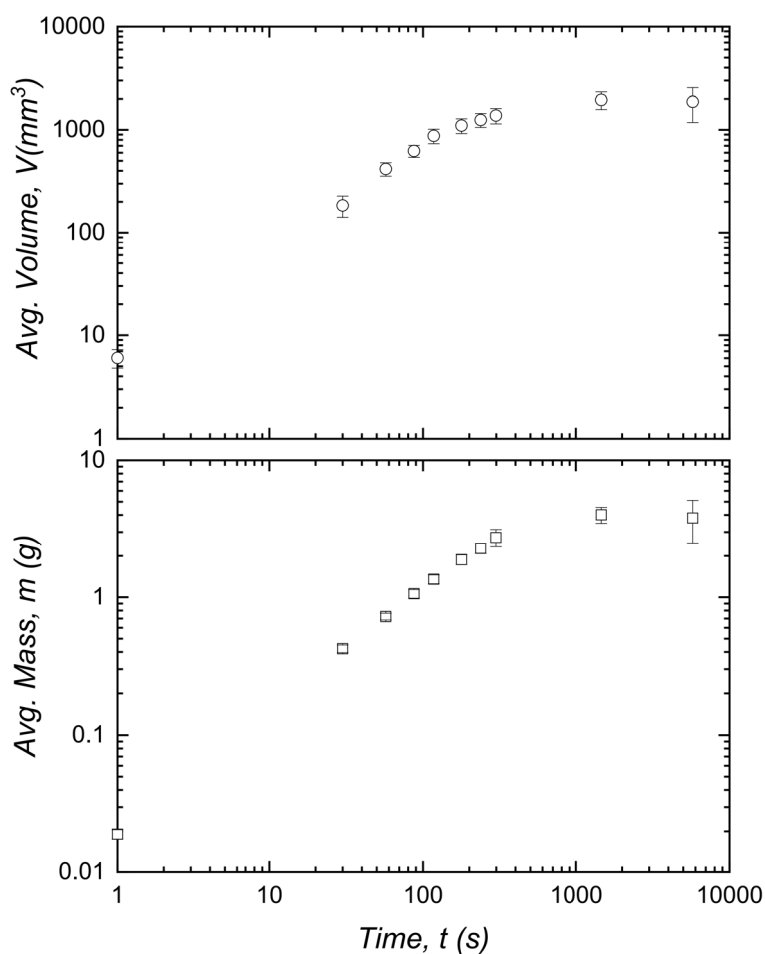
Figure 3.4: The mass and volume change of the hydrogel beads over time.

polymer to the weight of the water in the hydrogel. The polymer percent in the swollen hydrogel bead was 0.5% wt. polymer. This tiny fraction of polymer is able to hold a large amount of water, making the hydrogel an ideal substance to hold the large amounts of water

needed to simulate the amount of water present in cartilage.

3.1.4   Conclusions

The large amount of water in a hydrogel, also means that the pore size of the hydrogel is large. Mechanical testing of this hydrogel would likely show that the sodium polyacrylate hydrogel is brittle and unable to resist large forces before failure. Because cartilage is only 68% - 80% water [3], there is room to add different materials to increase the overall strength of the material. Other ways to increase the mechanical performance of the hydrogel would be to use a different polymer base chain as well as increasing the polymer percentage in the hydrogel. By adding materials to change the mechanical properties of hydrogels, a baseline measurement of a hydrogel with known properties to ensure the proper analysis is being conducted.

3.2   Agar Gel Testing

3.2.1   Introduction

Because hydrogels are suitable carriers for the amount of water that is needed in a composite material to replicate cartilage. By performing tests on gels that have already established data and are simple to fabricate, the viscoelastic and poroelastic analysis along with proper proceudre can be developed and implemented. Agar gels have been used in previous work for tissue engineering due to their simplicity and safety [1]. These gels are simple, because the only ingredients are agar and water. By adjusting the concentration of agar in the gel matrix, differences in the time-dependent response can be observed.

3.2.2   Methods

The agar gels were created in three different concentrations, 1%, 2%, and 3%. The powdered agar was obtained from Sigma-Aldrich (St. Louis, Mo. USA). Agar was weighed in the proper proportions and mixed with distilled water to create the proper solutions. To crosslink the agar, the solution was heated to 90° for a minimum of 10 minutes. The agar gels were poured into petri dishes to act as molds. Two separate gels were created from each solution for a

total of six gels. The gels were allowed to set inside of a 4.4°C refrigerator with a thin film of deionized water on top and wrapped in Parafilm (Bemis Company Inc. WI, USA) to ensure the gels are at equilibrium when testing and minimize the water lost to evaporation. The mechanical testing of the gels was conducted on a TA Instruments Electroforce 5500 (New Castle DE, USA). To configure the device for indentation testing an 8 mm diameter indenter
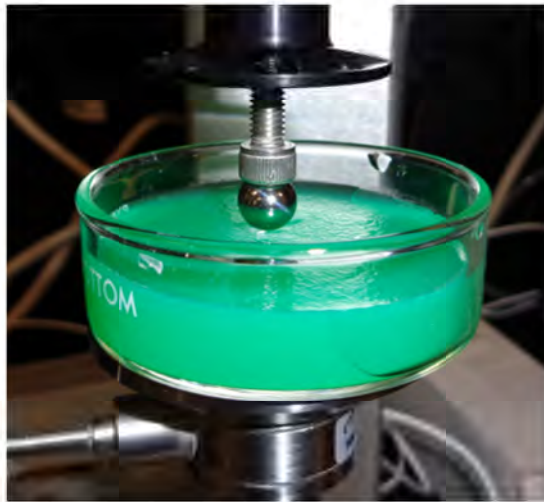
Figure 3.5: Photo showing an example setup for an indentation test with agar gels.

probe was fitted to the device along with a platen on the bottom to hold the petri dish with the agar gel. The expected strain of the material was calculated by using the indenter probe radius, R, and the indentation depth, h in Equation 15. The indentation depth for this experiment was 1 mm and the indenter probe radius of 4 mm, creates an expected strain of 10%. The test began with the machine finding the surface of the gel by moving down until a certain force, 0.025 N was read by the load cell. This then told the machine to stop for five seconds before the indentation began. The indentation took 5 seconds to complete and the relaxation time was 300 seconds. Each gel was tested a total of four times for a total of 24 tests. The location of the indentation site was also changed in between each test. The data was exported to R-studio (RStudio Inc MA, USA) for both viscoelastic and poroelastic analysis. For the viscoelastic analysis the initial guesses for the coefficients were given by solving the equation by assuming the end of the test, $t = 300s$, is $t = \infty$. Uusing the load data at that point to solve for C_0. Initial guesses of C_1, and C_2, were assumed to be 10% and 20% of C_0 respectively. The time constants τ_1, and τ_2, were estimated to be the rise time and

27
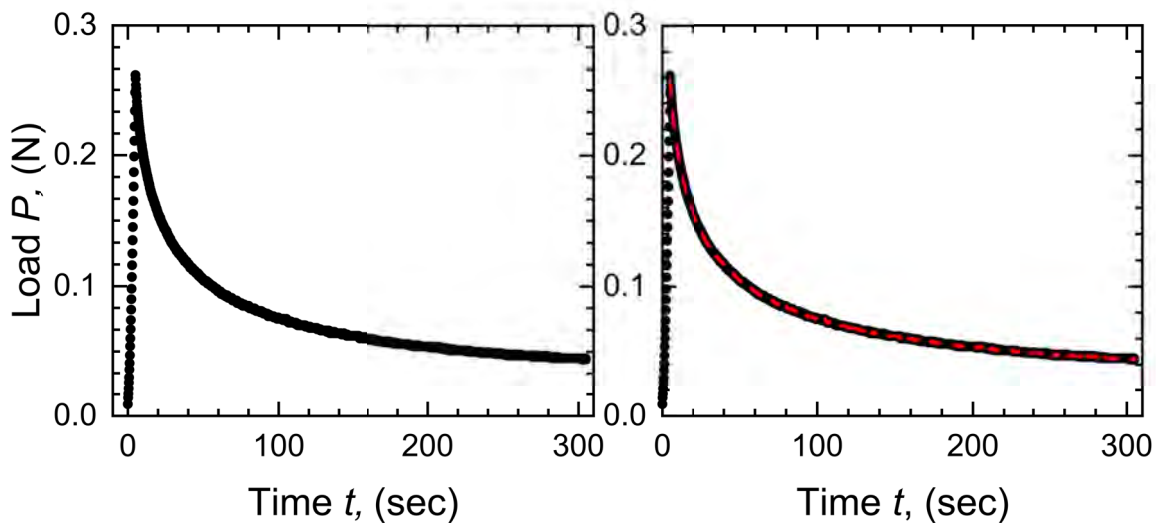
Figure 3.6: The load-time data output from the TA Electroforce 5500.

hold time respectively [1]. The least squares algorithm generated a curve that fit the data and the proper coefficients to input into the modulus calculation. The coefficients were then input into Equation 5 to find the elastic modulus as a function of time. The instantaneous and infinite shear modulus was also found, along with the viscoelastic ratio. Poroelastic analysis was conducted producing the shear modulus of the material, the permeability of the material, and Poisson's ratio.

3.2.3   Results

As expected, the 1% gel was the least stiff gel and the 3% gel is the most stiff. The values gathered from the viscoelastic analysis are reported in Table 1. The values for both the

Table 1: Agar Gel Viscoelastic Data

Gel Type	Instantaneous Shear Modulus, G_0 (kPa)	Infinite Shear Modulus, G_∞ (kPa)	Viscoelastic Ratio, (G_∞/G_0)
1% Agar	22.2 ± 3.8	3.8 ± 1.3	0.18 ± 0.016
2% Agar	67.8 ± 22.4	13.7 ± 4.5	0.20 ± 0.010
3% Agar	131.8 ± 43.9	25.1 ± 8.5	0.19 ± 0.013

instant and infinite moduli increase as the percentage of agar in the gel increases. The Standard deviation between the samples is also much larger for the instantaneous modulus

when compared to the infinite modulus. The transition from the instantaneous modulus to the infinite modulus follows an exponential decay curve and is shown in Figure 4.7. The
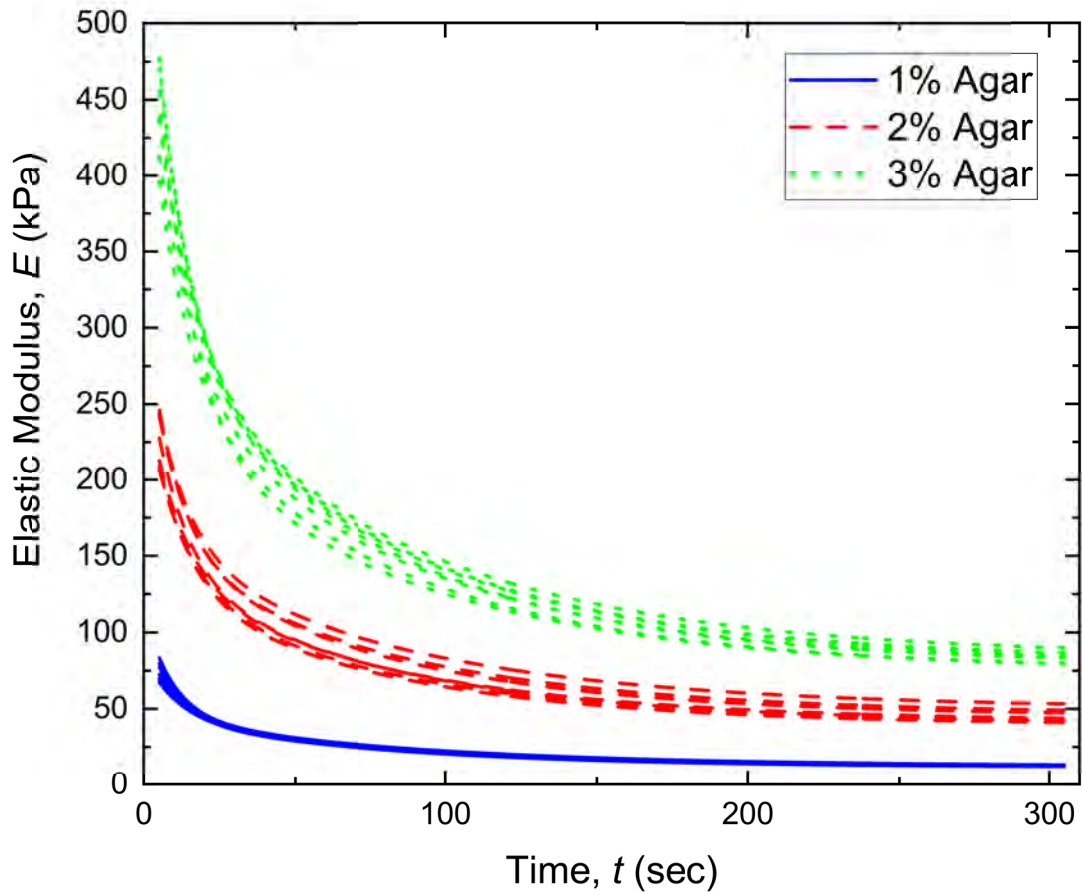
Figure 3.7: The curve generated by the algorithm imposed on the load-time data points.

polymer percentage is related to the square of the modulus and can be shown by fitting a quadratic curve predicting the modulus at polymer percent values in between those that were tested. Both the instantaneous and infinite shear moduli were used for this calculation. The results from poroelastic analysis is portrayed in Table 2.
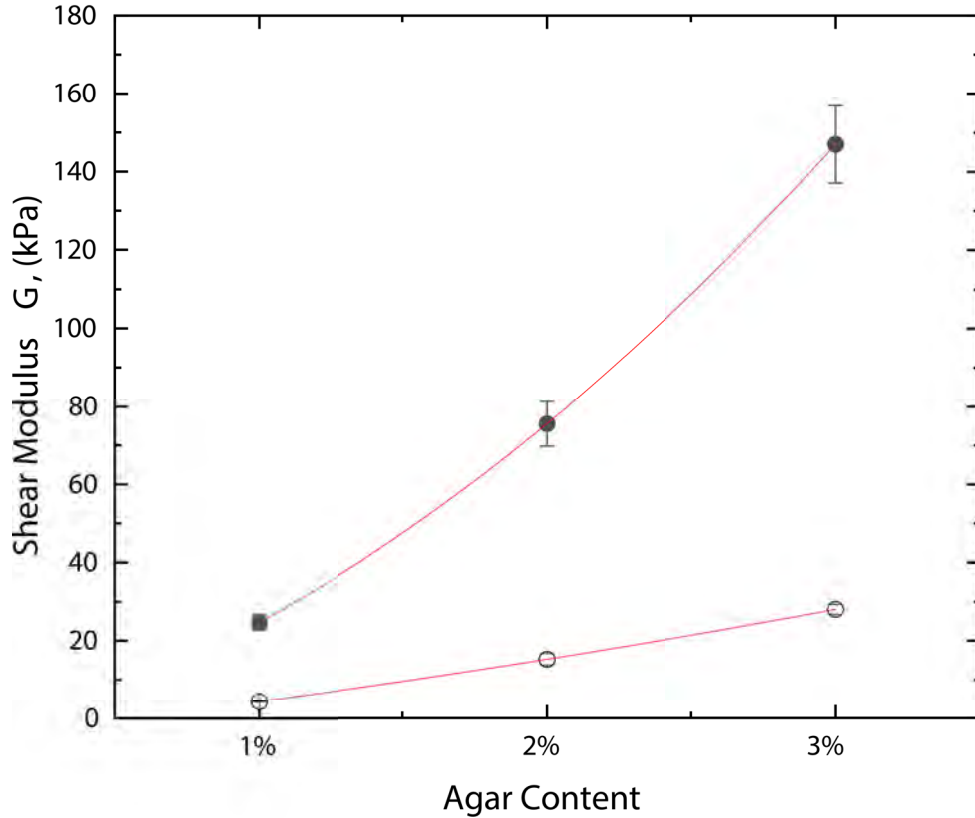
Figure 3.8: .
(A) The difference between the instantaneous shear modulus (closed dots), and the infinite shear modulus (open dots) for the different agar gels. (B) The viscoelastic ratio of G_∞/G_0.

Table 2: Agar Gel Poroelastic Data

Gel Type	Shear Modulus, G (kPa)	Permeability, κ (cm^2)	Poisson's Ratio, ν
1% Agar	26.6 ± 2.4	3.069E -12 ± 1.48E -13	-2.24 ± 0.38
2% Agar	80.8 ± 6.3	9.45E -13 ± 0.82E -13	-1.73 ± 0.14
3% Agar	158.0 ± 11.7	4.85E -13 ± 0.41E -13	-1.89 ± 0.23

3.2.4   Discussion

The agar gels are characterized as a poroviscoelastic material where the viscoelastic response dominates the behavior of the material [1]. Due to this, a viscoelastic assumption about the material is much more accurate and can be seen in the data by the viscoelastic analysis producing the expected change in modulus for the given gel percent in Figure 3.8. This is in agreement with previous data recorded from agar gels. Poroelastic analysis was also

30
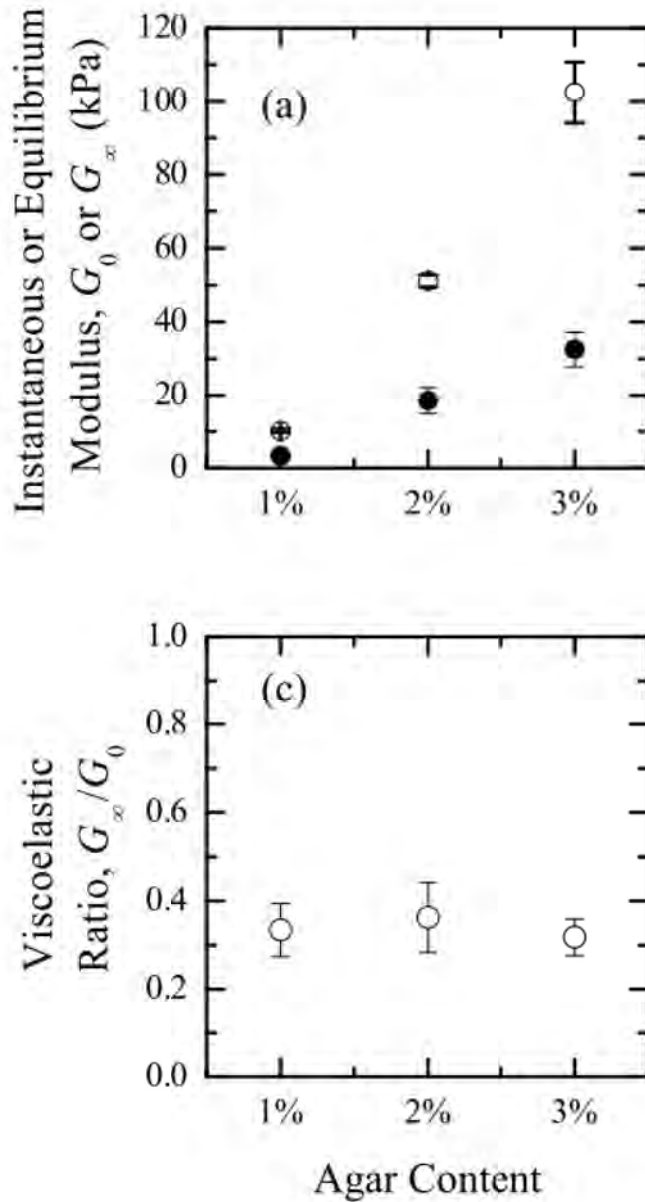
Figure 3.9: The shear modulus and the viscoelastic ratio for agar gels acquired from previous testing [1].

performed on the agar gels, but due to the viscoelastic response dominating the material behavior, this leads to inconsistencies in the poroelastic analysis. For example, the drained Poisson's ratio of the gels was determined to be less than -1. The is unreasonable because Poisson's ratio is bounded between -1 and 0.5. For Poisson's ratio to be outside of that range means that the initial assumption about poroelastic nature of the agar gels is incorrect. The Shear modulus values for the agar gels are reasonable, being in between the instantaneous and infinite values for the viscoelastic analysis of the shear modulus.

By taking previous 3% agar gel data some differences can be found in the stiffness, the stiffness of the previous testing was lower at 307.16 ± 24.93 for an instantaneous elastic modulus compared to 441.2 ± 29.8. These differences can be addressed in the experimental setup where in previous work, phosphate buffered saline was used as the testing solvent were de-ionized water was used for the work shown here [1]. The strains experienced by the gels are also different leading to differences from the non-linear response of the material.

3.2.5   Conclusions

From the testing conducted, the agar gels performed and behaved similarly to previous gels analyzed in both viscoelastic and poroelastic methods. There remains limitations to the accuracy of the results due to the trade-off between the simplicity of the poroelastic and the viscoelastic models and the error produced in the result. With a model that is easir to implement and use, the error is expected to be larger, especially for more complex multi-polymer gels that exhibit both poroelastic and viscoelastic characteristics. The true nature of the agar gels is reported as poroviscoelastic with a predominant viscoelastic behavior in shorter time scales where the poroelastic response dominates as the time scale grows larger [1]. The time scales used in this study kept the viscoelastic response dominant allowing for the viscoelastic analysis to produce more accurate results than the poroelastic analysis.

3.3   Ramp Time Testing

3.3.1   Introduction

The TA Electroforce 5500 mechanical testing instrument has not been tested to determine the optimal ramp time for the time dependent tests. The ramp time has an impact on the relaxation, because the instance that the force is applied the relaxation starts. To maintain an optimal test the ramp time is significantly shorter than the hold time. The issue with many mechanical testing devices is that the device will exceed the intended displacement if the ramp time is too small or not reach the desired depth by stopping short of the expected displacement. The purpose of this experiment is to investigate multiple ramp rates and

determine the optimal ramp time to allow for the smallest ramp time to lessen the effects of the ramp curve on the viscoelastic and poroelastic analysis.

3.3.2 Methods

For this experiment 2% agar gels were used in testing due to the simplicity of fabrication. Two gels were made and used for the testing. An 8 mm indenter was used for the experiment. The gels were loaded to a depth of 0.5 mm at varying rates. The different ramp times used were 0.1 s, 0.5 s, 1 s, 5 s, and 10 s. Each gel was loaded twice resulting in four tests for each ramp time. The test was setup in a manner such that a 0.020 N pre-load was found before a hold time of 5 seconds with the ramp following after. The peak load and the error from the expected indentation depth were recorded.

3.3.3 Results

For the slowest ramp time, ten seconds, the error was negligible at 0.2 ± 0.16%. The five second ramp time had a similar error at 0.35 ± 0.1%. The one second and point-five second ramp times shared similar amounts of error at 1.05 ± 0.1% and 2.25 ± 0.1% respectively. The only ramp time that had significant amounts of error was the point-one second ramp time at 10.65 ± 0.44.

Table 3: Ramp Data

Ramp Time, s	Actual Displacement, mm	Percent Error	Peak Load, N
0.1	0.447 ± 0.086	10.65 ± 0.44	0.561 ± 0.099
0.5	0.489 ± 0.104	2.25 ± 0.10	0.603 ± 0.121
1	0.495 ± 0.043	1.05 ± 0.10	0.573 ± 0.050
5	0.498 ± 0.063	0.35 ± 0.10	0.552 ± 0.073
10	0.499 ± 0.093	0.2 ± 0.16	0.538 ± 0.107

3.3.4 Discussion

One of the fundamental understandings of science and more specifically engineering is that the accuracy of your measurements depends on the reliability of the machine used to make those measurements. Here, the testing of different ramp times is important due to the nature

of biological tissues. Many of these tissues such as cartilage are strain rate dependent [3,26]. By testing here and choosing a strain rate that is consistent with the abilities of the equipment to use for future experiments. The decision was made to use strain rates smaller than 1 mm/s as to not introduce large amounts of variance in the actual displacement of the test. Even though the maximum depth can be changed from experiment to experiment, removing this variable from future testing increases the accuracy of the measurement and tries to eliminate extraneous variables that can impact the measurement being recorded.

3.3.5   Conclusions

Repeatability and reliability are foundations of good science. By investigating what errors are introduced from making measurements, sources of error can be diminished. Using a constant strain rate in indentation testing can increase the repeatability of a measurement and give value to the measurements that are made in the future. Another way to reduce the amount of error in a study is to perform the same experiment on a common, known, material. Fracture testing is a complex field and by testing on a simple material error can be further reduced.

3.4   Mechanical Testing of Paper

3.4.1   Introduction

When examining a material, multiple methods of observation allow for a more thorough understanding of the material. By only using a single measurement to define how a material behaves there is a lot of information that is lost. Two such parameters that must be considered are the strength and toughness of a material. These two parameters are generally opposed to each other meaning that if a material is more tough, it is generally not as strong. Toughness is defined as the energy needed to propagate a crack in a material where as the strength is the stress at which a material will fail. Materials are generally either strong or tough with a select few materials being both. The Strength versus Toughness plot above shows the wide range of of different materials. Metals are generally categorized as being both tough and strong while foams are generally weak in both categories.
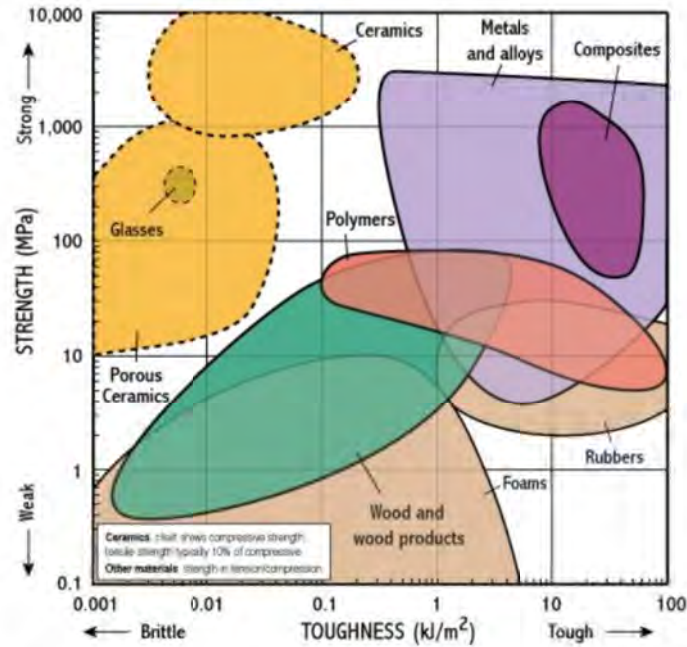
Figure 3.10: Plot of the strength versus toughness for a variety of materials. Taken from: http://www-materials.eng.cam.ac.uk/mpsite/interactive_charts/strength-toughness/NS6Chart.html (Date Accessed: March 1st, 2020)

To determine the toughness and strength of the composite material proposed earlier, testing on a surrogate material needs to be completed in order to build proper procedure for analyzing both the strength and toughness of a material. To determine the toughness, mode III, also referred to as a trouser tear test was chosen as to isolate the energy going to propagate the crack in the material. By placing the material in mode III, the energy put into deforming
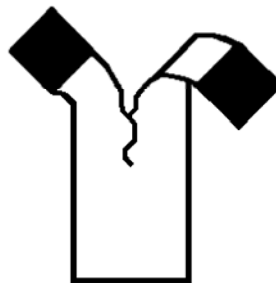
Figure 3.11: Schematic of mode III testing.

the material is minimized and the energy propagating the crack is maximized. Equation 13

35

in Section 2 assumes that there is no deformation in the material as the material fractures. This is important to take into account because of the time dependent effects seen in biological materials along with the large strains experienced during testing.

Measurement of the strength is also more difficult with biological tissues. Due to the expected thickness of the composites, about 0.5 mm, indentation will not be enough to characterize the stiffness or the elastic modulus of the material. By performing a simple tensile test, both the strength and stiffness of the material can be captured. Because the samples of paper are so thin, there is little deformation along the z-axis of the material along with the expected stress at failure. When testing steel, direct measurements of the strain are needed because both the grips and load cell are made of similar material meaning that they also undergo some amount of deformation due to the load being propagated through the whole machine. The expected force on the order of Pa and not MPa means that the equipment on the TA Electroforce 5500 will not deform and require a direct measurement of the strain during tensile testing.

With the types of testing now chosen, a suitable material needs to be acquired to perform the preliminary testing with. The ideal material would be easy to obtain, cheap, non-toxic to work with, and similar in size to the composites that will be tested later. Paper was chosen because it is widely available and has a structure that is similar to a fiber reinforced composite.

3.4.2 Methods

Imaging of the specimens was conducted on a Zeiss EVO 10 scanning electron microscope (SEM, Oberkochen, Germany). The samples were sputter coated to improve image quality. Images were taken at 5000 times magnification.

Two types of paper were obtained for this experiment. White printer paper and blue craft paper were used. A 3D printed guide was used to cut the paper into 25 mm x 10 mm rectangles. For fracture testing six samples were used for each group, while for tensile testing, ten samples were used for each group. Mode III tear fracture "trouser-tear" tests
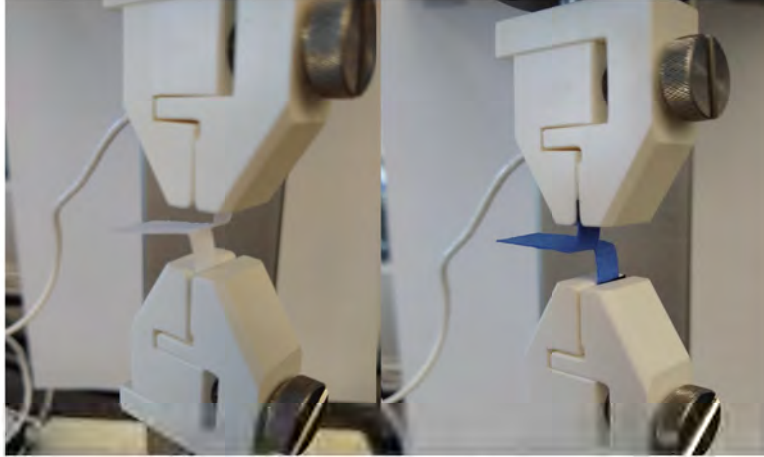
Figure 3.12: Setup of the white paper, shown on the left, and the blue paper, shown on the right, in mode III fracture

were conducted using a TA Instruments Electroforce 5500 with a 25 N load cell. Metal grips were supplied by the instrument manufacturer. Specimens were 10 mm wide and 30 mm long, and an initial notch of 5 mm was introduced. The specimens were torn at 0.5 mm s^{-1} such that each test lasted a total of 20 seconds and resulted in a crack length extension of approximately 10 mm. The thickness t of each specimen was determined with calipers (Gyros DIGI-SCIENCE Accumatic Digital Electronic Caliper, Monsey NY, USA) by multiple measurements prior to each test. The average load (P_0, Figure 1) was used in conjunction with the sample thickness to calculate the tear toughness T_c as in Equation 3. Fracture analysis uses an average load to determine the fracture toughness. To achieve this the load-time data was parsed by looking for the change in the first derivative from a positive value or zero value to a significant negative value chosen to be -0.5. This was chosen because a slope of -0.5 ensures that the data is following a negative trend and is not noise from the machine. By eliminating 80% of the data prior to the slope change the load rise curve was not taken into account when calculating the average load for fracture.

3.4.3 Tensile Testing

Blue craft paper and white computer paper were obtained and cut into 25 mm by 10 mm rectangles. The samples were then marked at 2.5 mm and 23.5 mm with a marker to ensure correct placement in the grips during testing. A total of 10 samples of each type of paper
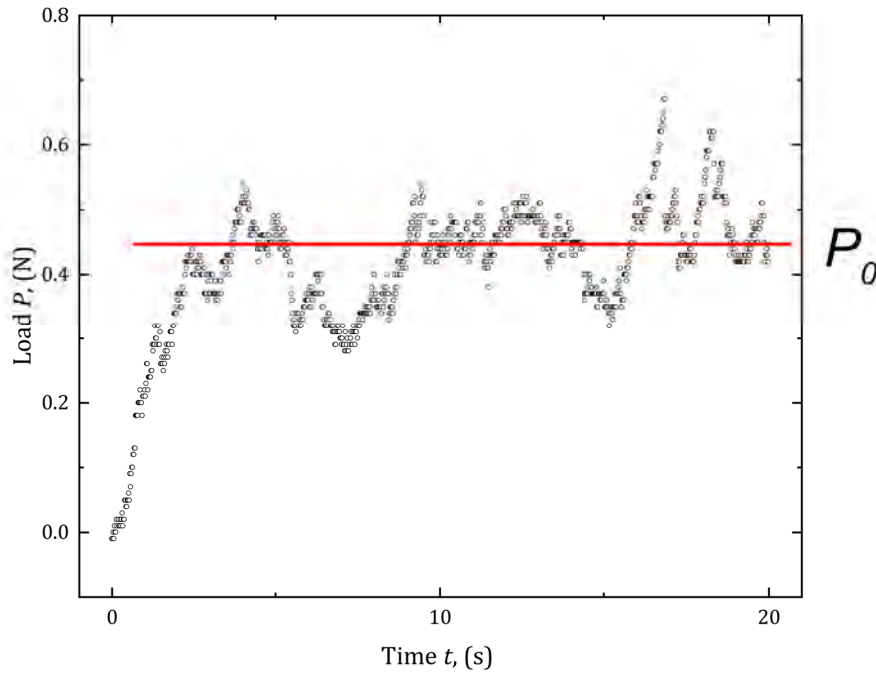
Figure 3.13: Load-time data for the fracture of blue paper.

were tested. Testing took place on the TA instruments Electroforce 5500. The test took place over 5 seconds, with the samples being loaded at a rate of 0.5 mm/s. Due to the high expected force of the tests, the 200 N load cell was used for the experiment. Before testing, the samples were measured using a pair of calipers to measure the thickness of each individual sample. The elastic modulus, strain energy density, failure strength, and ultimate tensile strength were calculated. The strain energy density was calculated as the area under the stress-strain curve and the ultimate tensile strength is defined as the peak stress experienced by the material.

3.4.4 Paper Imaging

The white paper was observed to be less stiff than the blue paper. Most likely due to the fact that the white paper was noticeably more thin. The blue paper had fibers that were visible to the naked eye without any magnification. Once image in the SEM, the white paper had a material on the individual fibers. This is assumed to be a type of glue used in the paper

38

White Paper   Blue Paper
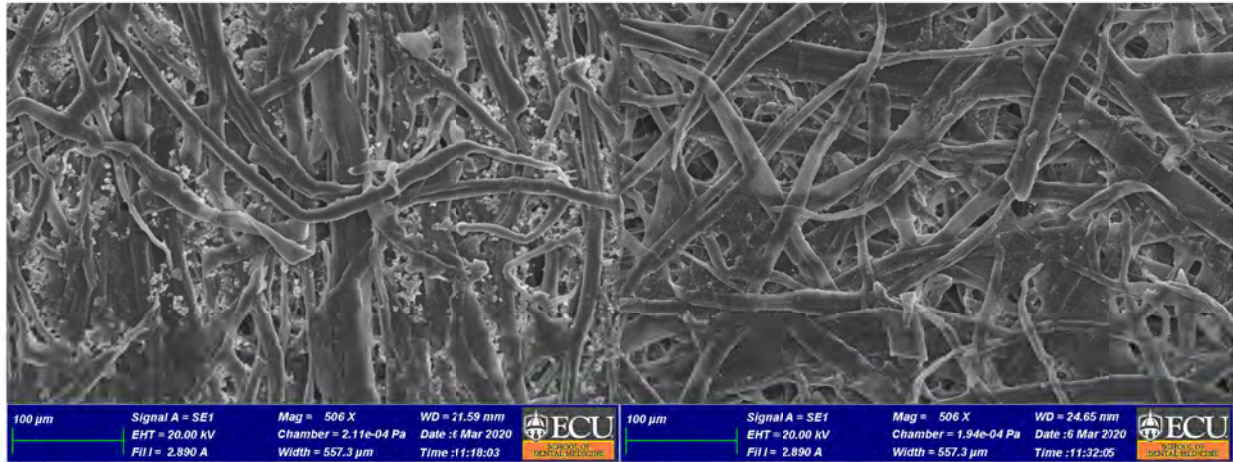
Figure 3.14: Image of the two types of paper, white computer paper and blue craft paper in their pristine condition.

making process. The images of the paper after failure show that the fibers have become

White Paper Failure Reigon   Blue Paper Failure Reigon
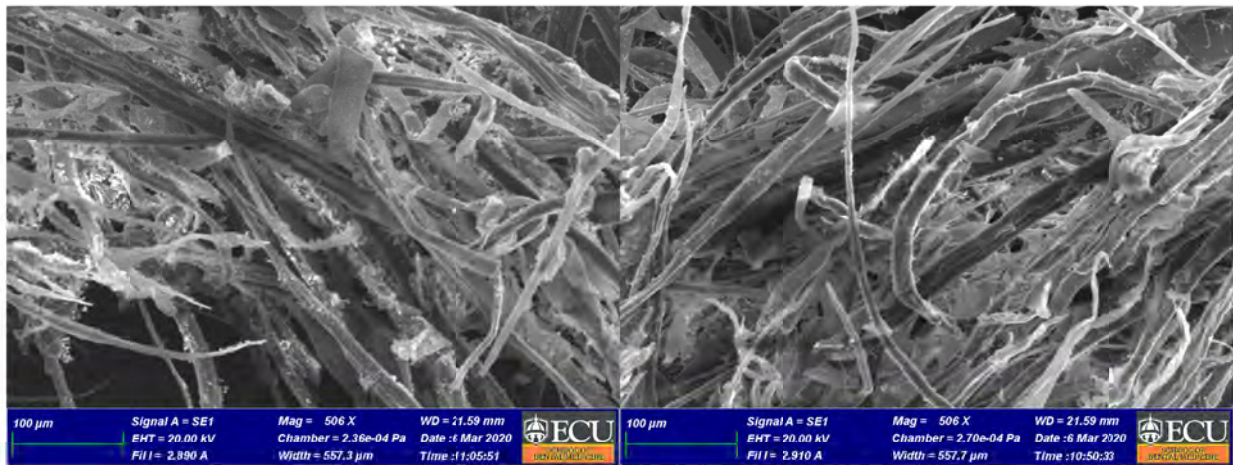
Figure 3.15: SEM images of the fracture regions of both types of paper after testing.

frayed and disassociated from each other.

3.4.5 Fracture Results

Despite being twice the thickness of the mean energy required for fracture for the blue paper was half of the energy required for the white paper. The blue paper also was more

consistent during testing expressing a smaller standard deviation at 1800 Jm^{-2} compared to the standard deviation of the white paper at 3400 Jm^{-2}.
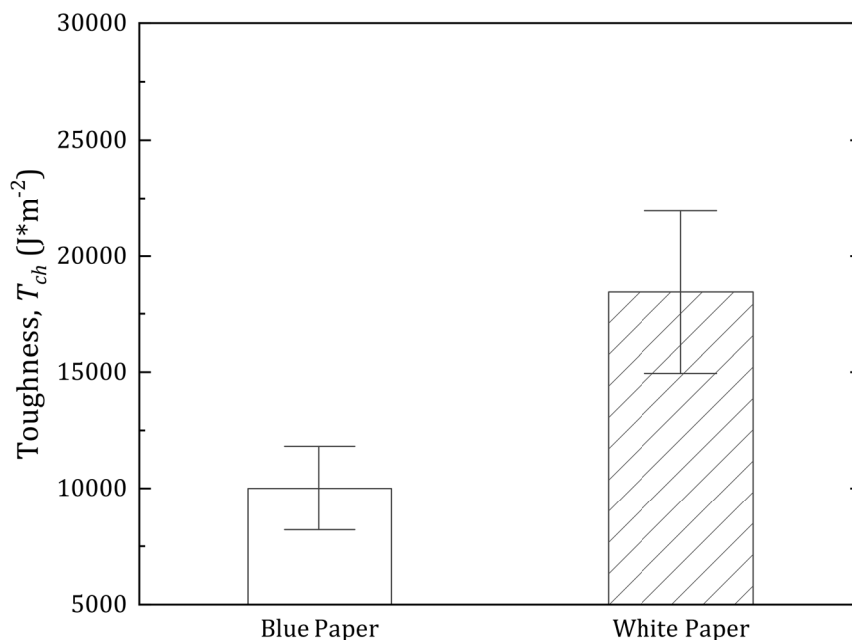
Figure 3.16: Comparing the fracture toughness for white paper and blue paper.

3.4.6 Tensile Results

The elastic modulus of the samples was calculated from the testing as the slope of the loading curve from the stress-strain data. An example of such can be seen in Figure 3.17. The results of the testing is shown in Table 3.

Table 4: Paper Tensile Data

Paper Type	Elastic Modulus, E (GPa)	Ultimate Tensile Strength, MPa	Failure Strength, MPa	Strain Energy Denstiy, $\frac{kJ}{m^3}$
Blue	4.06 ± 0.52	53.1 ± 3.5	51.3 ± 3.6	29.3 ± 5.5
White	2.16 ± 1.46	27.9 ± 12.9	26.7 ± 13.6	26.6 ± 4.38
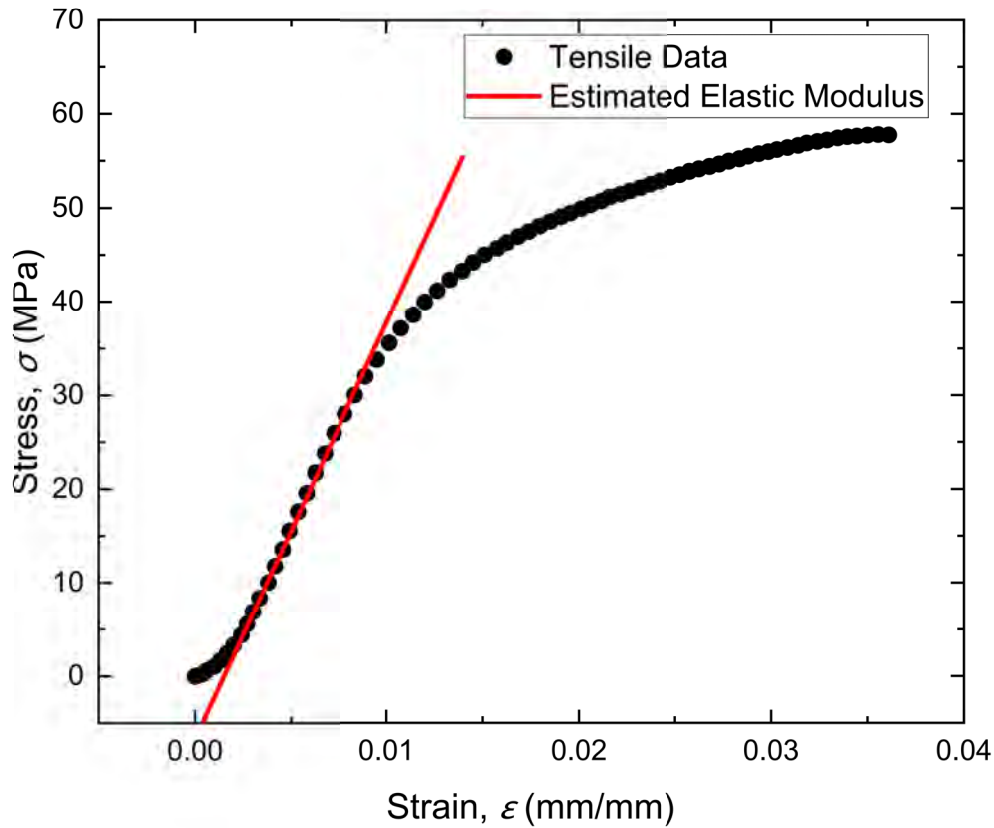
Figure 3.17: Stress-Strain curve with the line used to estimate the elastic modulus.

3.4.7 Discussion

The difference between the blue and white paper comes from the type of paper used. The blue construction paper had a much larger grain and individual fibers could be seen even without a microscope. While the white paper did not have any visible fibers leftover from production. These visible fibers on the blue paper are important because they can be a possible explanation as to why the white paper has a higher toughness despite being thinner than the white paper. These fibers in the white paper are most likely a result of the manufacturing process and the size of the pulp used to create the paper. Paper, a product of cellulose, the cell walls of plant cells, can be likened to the gelatin that is made from the connective tissue and unused parts of animals. This similarity also introduces the question of the possibility of time dependent effects. The tests performed here are at a low strain rate $0.5 \ mm/s$.

Common industry practice for testing paper is at high strain rates using a gravity powered device that fractures the material in a manner resembling a Charpy impact test [27]. Due to the nature of biological materials it would not be surprising to see strain rate dependent effects on a material such as paper. The investigation of this is unfortunately out of the scope of this work but could prove to be beneficial in the future to the development of interesting fiber reinforced composites using cellulose as the fibrous material. Future Fourier-transform infra-red Spectroscopy could divulge the information as to what the material is that is on the white paper. From industry practice it could be chalk to increase the white color of the paper or something else dependent on the manufacturer [27].

3.4.8 Conclusions

Here, the difference between the strength and toughness of two different types of paper, blue construction paper and white printer paper are analyzed. The testing here allows the production of a set of methods that can be used in the future testing of the composite material and their components. Paper is an interesting material and its potential applications for something more than its common use as a material to print and write on. Paper also shares a common structure with electrospun fibers. With both being materials made up of randomly oriented fibers. This commonality allows the easy transition from testing paper to testing electrospun fibers.

4 Electrospun Fibers and PVA Hydrogels

4.1 Electrospun Fiber Fabrication and Testing

4.1.1 Introduction

Electrospinning has seen a rise in popularity due to its ability to create fibers on the scale of those inside of the body [17, 20, 21]. One issue in the implementation of electrospun fibers is that of crosslinking. Crosslinking electrospun fibers is there to impart water stability and increases the stiffness of the mat by creating additional bonds between single chains [28, 29]. The fracture properties of these fibers has not been investigated and needs to be understood before inclusion into the composite material. With the charged ions and hydrogel in the composite, it is important to be able to understand the contributions that the electrospun fibers will add to the composite.

4.1.2 Methods

For uncrosslinked fibers, gelatin at 12 wt.% was dissolved in 9:1 by weight acetic acid (¿99.7% VWR PA, USA) and distilled water. The solution was used for electrospinning within a week of creation. For crosslinked fibers, citric acid (Sigma-Aldrich MO, USA) and sodium hypophosphite (SHP) (Sigma-Aldrich MO, USA) were added to the gelatin-acetic acid-distilled water solution prior to crosslinking at 15% citric acid and 7.5% SHP respectively [29]. A SprayBase A001 20kV electrospinning kit (Co. Kildare, Ireland) was used to produce the nanofiber mats on a static collector at a working distance of 12 cm. The working voltage was 11 kV and the collection lasted 7 hours per mat. Fiber mats containing the citric acid and SHP were crosslinked in a 150 °C oven for four hours after holding in a desiccator prior to and following crosslinking. Plain gelatin mats were stored in a dessicator until imaging or mechanical testing. A Zeiss EVO 10 scanning electron microscope (SEM, Oberkochen, Germany) was used to image fibers in the as-fabricated state and following mechanical testing. Squares of 5 mm x 5 mm were taken from both the uncrosslinked and crosslinked sheets for imaging after fabrication. After fracture testing, a second group of fiber mat specimens were imaged at the crack tip. All fiber mats were sputter-coated prior to imaging with silver in a
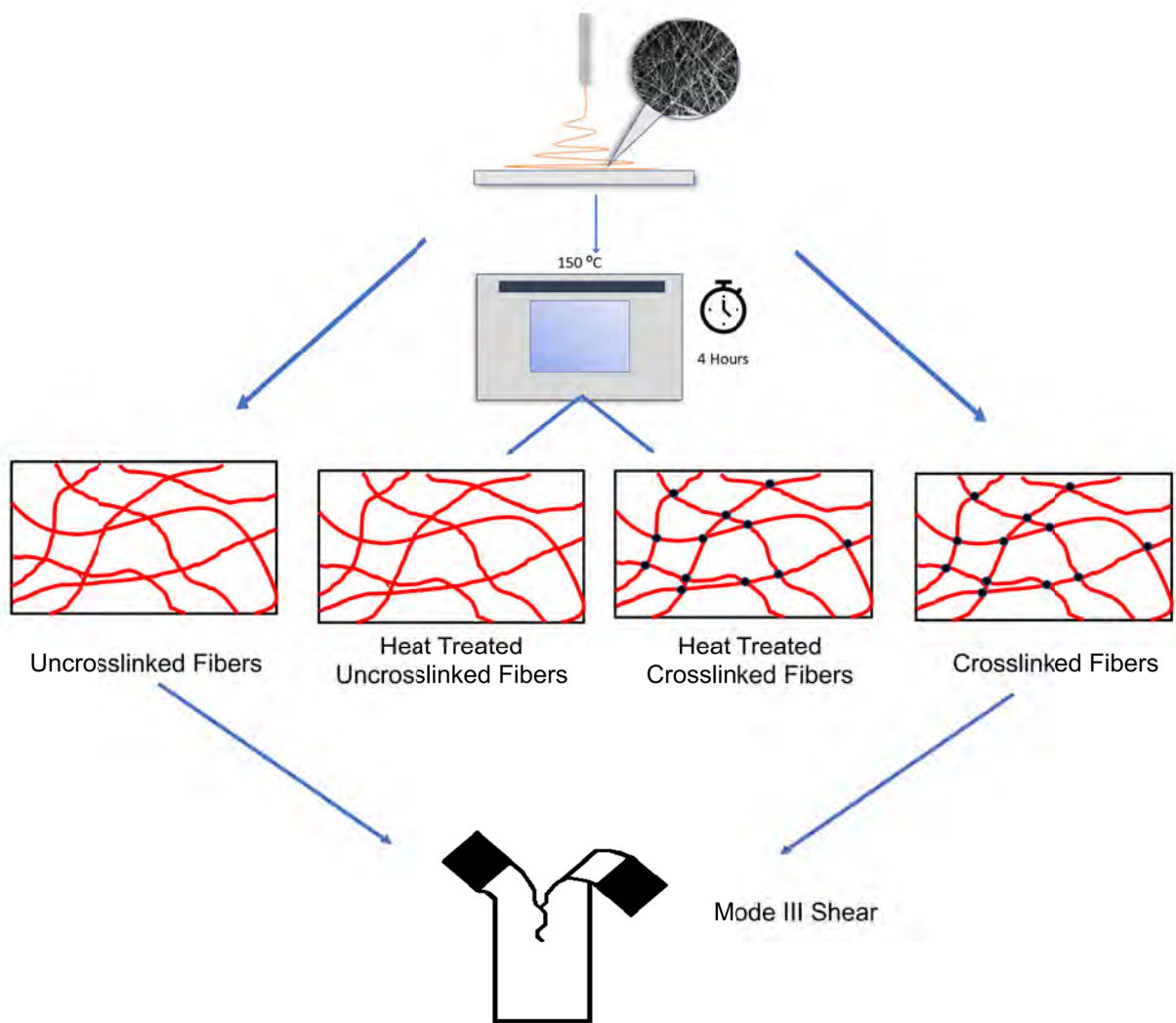
Figure 4.1: Experimenting with the electrospun fibers involved a three-step process. Manufacture via electrospinning, crosslinking where relevant, and mode III testing.

Denton Vacuum Desk V (Moorestown NJ, USA) at 50 mA for 60 s. Mode III tear fracture ("trouser-tear") tests were conducted using a TA Instruments Electroforce 5500 with a 25 N load cell. Metal grips were supplied by the instrument manufacturer. Specimens were 10 mm wide and 30 mm long, and an initial notch of 5 mm was introduced. Specimens, 10 per group, were torn at 0.5 mm s^{-1} such that each test lasted a total of 20 seconds and resulted in a crack length extension of approximately 10 mm. The thickness t of each specimen was determined with calipers (Gyros DIGI-SCIENCE Accumatic Digital Electronic Caliper, Monsey NY, USA) by multiple measurements prior to each test. The average load

Figure 4.2: Setup for the electrospun fiber mat testing on the TA Electroforce 5500 with metal grips attached.

(P_0, Figure 3.13) was used in conjunction with the sample thickness to calculate the tear toughness T_c as in Equation 13.

4.1.3 Results

After fabrication the two fiber mat groups, crosslinked and uncrosslinked, exhibited different tactile qualities. The uncrosslinked group felt less stiff and exhibited a more cloth-like appearance and texture. This treatment also resulted in a slightly higher mean thickness for the uncrosslinked fiber mats compared to the crosslinked fiber mats, h = 0.206 ± 0.069 mm versus h = 0.193 ± 0.045 mm. The crosslinked fiber mats also appeared to be an off-white color, while the uncrosslinked fibers were plain white. Figure 2 presents SEM images of the as-fabricated fiber mats in both conditions. The differences in these two fiber mat groups due to crosslinking can also be seen in the raw load-time (P-t) data from the mode III fracture tests (Figure 4.7). The P-t data for uncrosslinked mats (Figure 4.7A) shows a gradual nonlinear response prior to the initiation of crack propagation (i.e. first load drop) while for crosslinked mats the rise to peak force is rapid and approximately linear (Figure 4.7B). The tear toughness of the two sets of fiber mats can be seen in Figure 4.8A. The average values for the uncrosslinked fiber mats was 396 ± 240 Jm^{-2} while the crosslinked fiber mats exhibited approximately double the mean tear toughness, 791 ± 242 Jm^{-2}. Figure 4.8B illustrates the slight increase in tear toughness values for the uncrosslinked mats depending

Uncrosslinked   Crosslinked
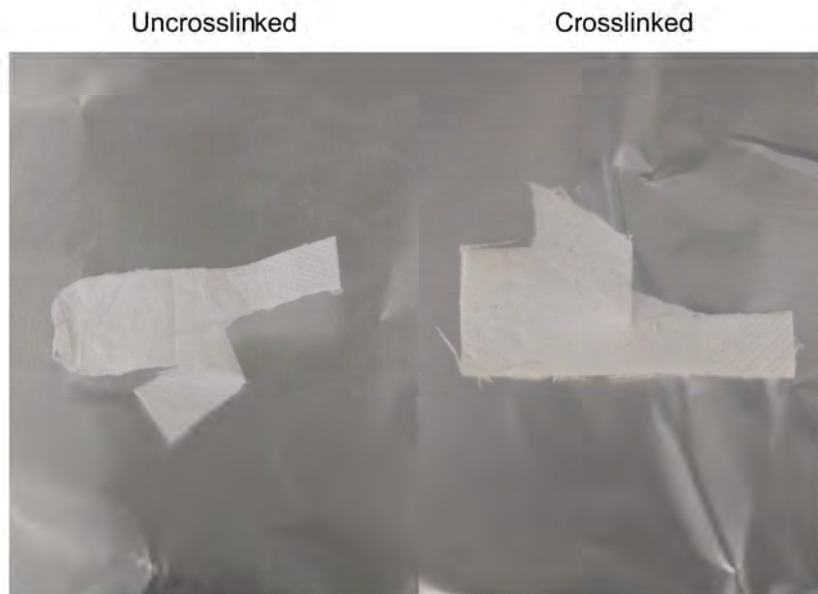
Figure 4.3: Example of both the uncrosslinked and crosslinked fibers after testing.
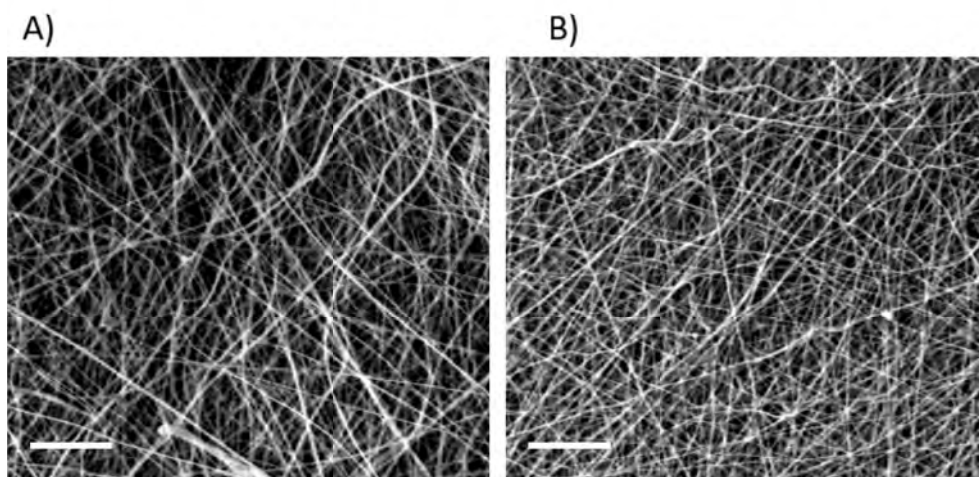
Figure 4.4: (A) Uncrosslinked gelatin fibers after fabrication. (B) crosslinked gelatin fibers after fabrication. Scale bar in each image is 20 μm.

on the portion of the load-time curve analyzed. There was a consistent increase in the toughness values with increased crack length for these specimens, a phenomenon that was not observed for the crosslinked specimens.

4.1.4 Discussion

In this study, electrospun gelatin nanofibers were compared in native (uncrosslinked) and crosslinked states and found to be tougher by about a factor of two when tested for mode
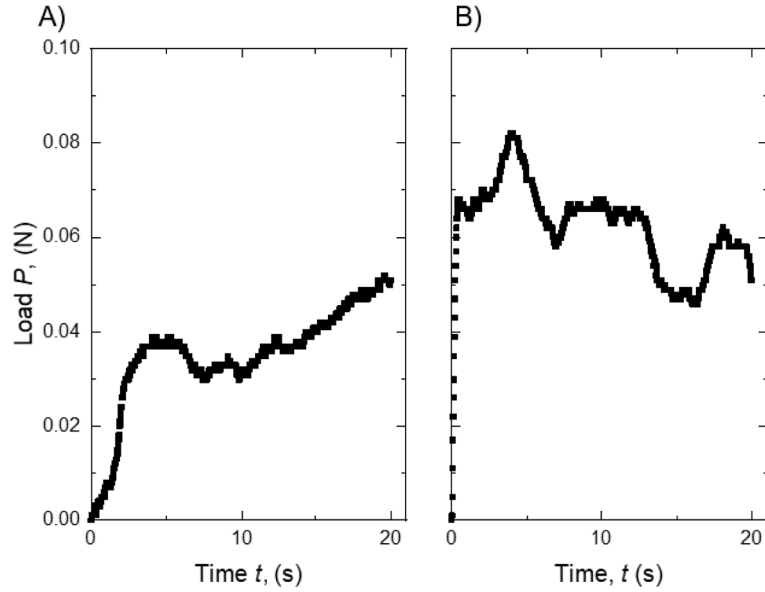
Figure 4.5: (A) An example load-time plot for one of the uncrosslinked fiber mats. (B) Load-time data from one of the crosslinked fiber mats.
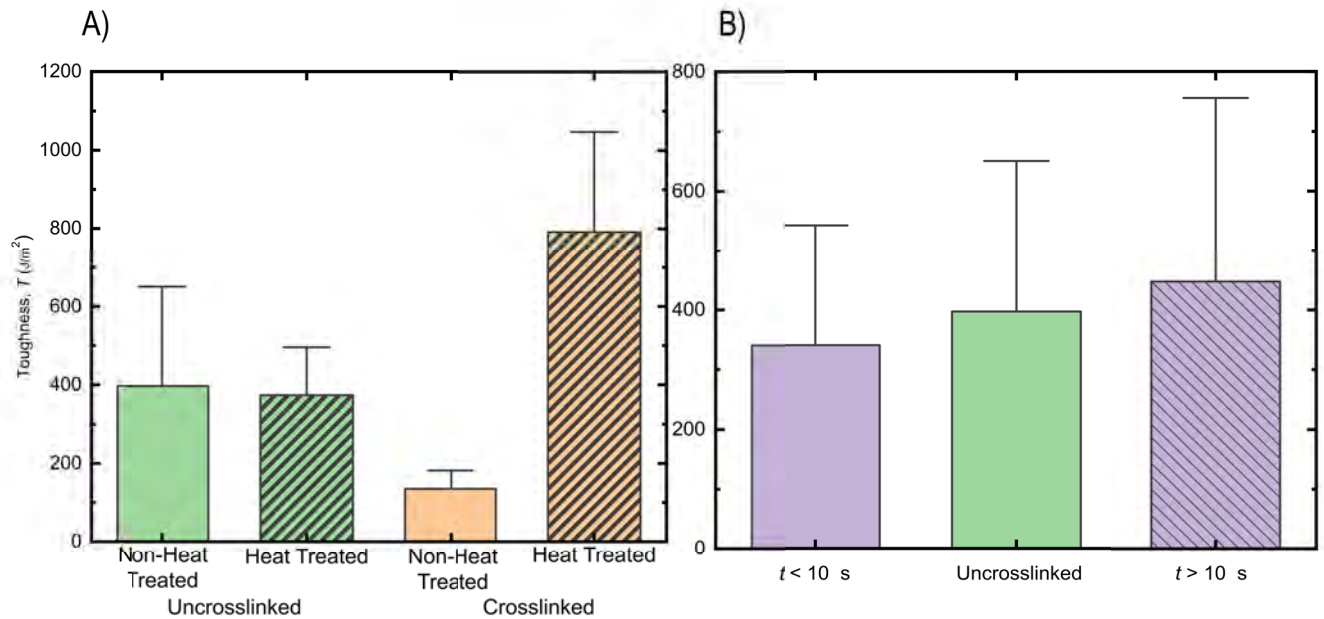
Figure 4.6: Tear toughness (T) values for (A) crosslinked vs uncrosslinked fiber mats and (B) uncrosslinked fiber mats analyzed from different portions of the load-time $(P - t)$ plot, demonstrating increased tear toughness with increased crack length.

III fracture. This increase in toughness is imperative for the purpose of creating a robust biomimetic artificial cartilage. In previous work, uncrosslinked gelatin fibers were embedded in a neutral hydrogel matrix, in an application envisioned for corneal tissue engineering [16].
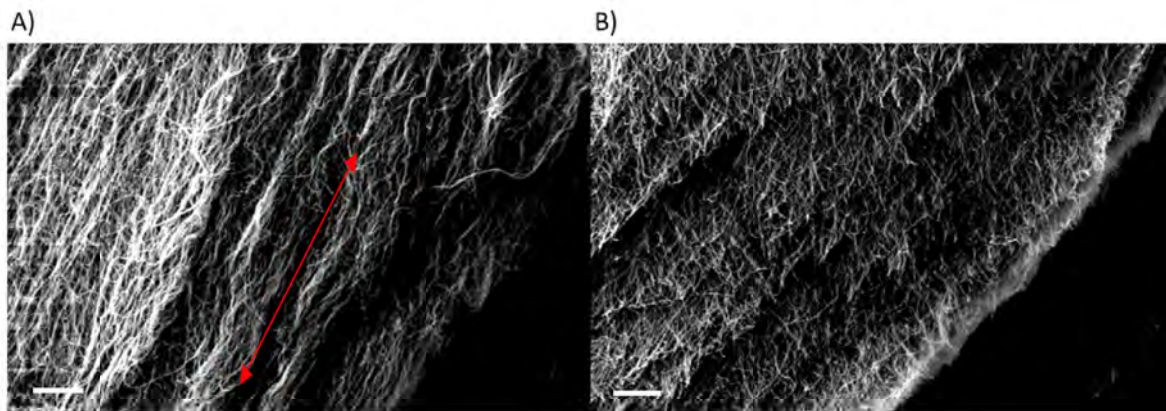
Figure 4.7: (A) SEM image of the uncrosslinked fiber mat after testing. The red arrow showing the direction of the load. (B) SEM image of the crosslinked fibers after testing.

In separate work, charged, polyelectrolyte gels were examined for their mechanical similarity to natural cartilage [5]. In order to make a truly biomimetic cartilage scaffold, both approaches will be combined, to include the inclusion of nanofibers mimicking collagen in a charged hydrogel mimicking the polysulfated proteoglycan ground substance in native cartilage.

The challenge in this biomimetic approach lies in the competing mechanical phenomena that arise from the different individual components of this complex natural composite. The negative charges provide stiffness to the tissue, since the fixed charge density is large. However, the proteoglycan network containing the charges is constrained within the collagen network, putting demanding tensile pre-stresses on the collagen. It is for this reason that the current study considered crosslinking of the gelatin nanofiber mats prior to hydrogel infiltration, resulting in a factor of two increase in the tear toughness. This relatively simple crosslinking approach, adopted from the literature [29], does not have the potential toxicity associated with more harsh crosslinking chemicals.

4.1.5   Conclusions

Investigation on the fracture properties of uncrosslinked versus crosslinked fiber mats showed that the treatment improved the toughness of the fiber mats while also imparting a resistance to swelling from water. This allows for the crosslinked scaffolds to be used in the composite

interacting with the large amounts of water that will be present. With the fibers fabricated and tested, the other major component of the composite, the hydrogel, can be investigated.

4.2 Low Molecular Weight PVA Hydrogels

4.2.1 Introduction

Poly (vinyl alcohol) and poly (acrylic acid) hydrogels have been shown to produce stable gels that have an active charge component inside of them [5,30]. These gels are water stable and have the crucial ionic component that has been missing in previous work to create tough hydrogels for articular cartilage repair or replacement. This charge component is critical for increasing the compressive stiffness of the material and replicating cartilage.

4.2.2 Methods

The gel composite is composed of a 3:1 ratio of 15% wt. PVA (M_w 31,000-50,000) (Sigma-Aldrich MO, USA) and 15% wt. PAA (M_w ~450,000) (Sigma-Aldrich MO, USA) respectively. Combined in a beaker, the two solutions are mixed until homogeneous. Once prepared, the mixture is poured into silicone bread molds and placed into the freezer. A single freeze thaw cycle consists of 8 hours in a -20 °C freezer followed by 4 hours at room temperature, about 23 °C. To create activated gels with charges in the matrix, the gels are placed in a 0.1 M sodium hydroxide solution until equilibrium is reached, about 48 hours. The sodium hydroxide solution is drained and the gels are rinsed repeatedly with water to bring the pH of the gels down to a safe level for testing. The gels were tested within 48 hours. The gels are tested on platens coated with waterproof sandpaper to prevent sliding during the indentation testing. Fracture testing was also considered using the same methods described in Chapter 3.4.

Testing of the gels was conducted on the TA electroforce 5500. An 15.9 mm spherical indenter probe was attached to prepare for indentation of the material. The ramp time of the test was 5 seconds to a depth of 1 mm. The hold portion of the test is 300 seconds a single gel was tested four times and analyzed using poroelastic analysis. A total of two gels

were tested and indented four times.

4.2.3 Results

The gels made were semi-transparent. An example of one of the gels made is shown in Figure 4.2, the gel shown here was used for indentation and gels similar to it were attempted to be used for mode III trouser tear tests. The gels used for the trouser tear tests we unable to
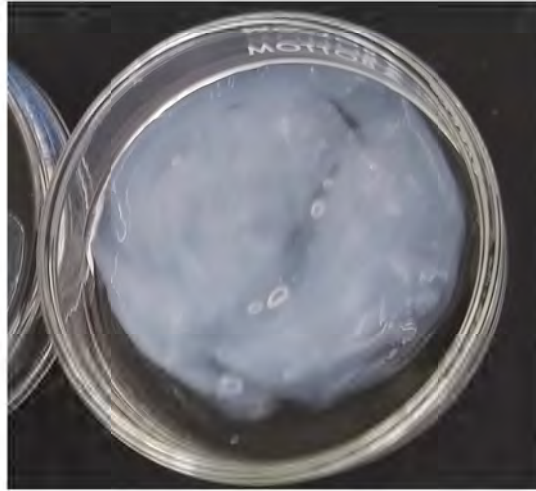
Figure 4.8: A PVA-PAA gel used for indentation.

hold their own weight and fell apart before being placed in the machine. This did not allow for the collection of any fracture data on the PVA $(M_w31{,}000\text{-}50{,}000)$-PAA$(M_w\text{~}450{,}000)$ gel. The load time data for one of the tests is also presented. This shows that the noise in the machine comprises a significant portion of the variance in the data collected. From this data, poroelastic analysis revealed that the shear modulus of the gels was 12.9 ± 1.3 kPa, Poisson's ratio at 0.384 ± 0.00505, and the permeability at $2.55^{-13} \pm 2.5^{-14}$ m^2.

4.2.4 Discussion

The results presented here fall short of those presented in the previous work performed by Offedu et al 2017. The reported value of the shear modulus of the PVA-PAA gel is around 30 kPa, the values here are about half of that at 13.2 kPa. This is more than an order of magnitude in difference from the values of cartilage [3]. This also does not take into account the issues with the viscoelastic analysis and the data recorded from the TA instruments
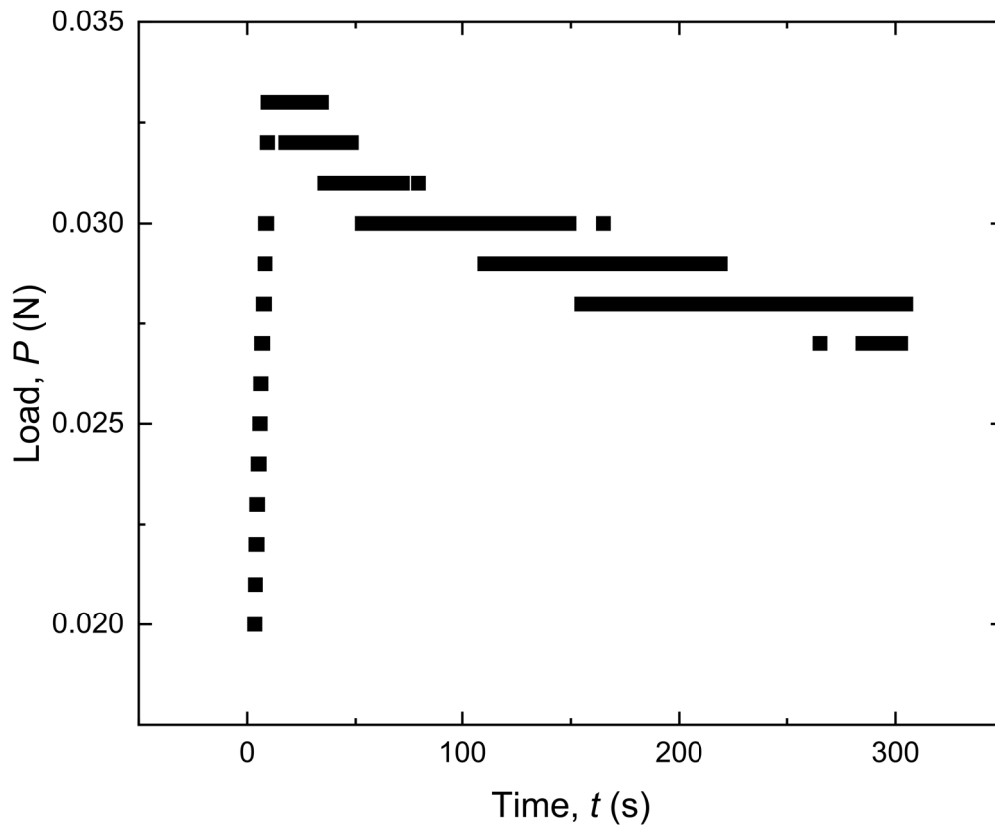
Figure 4.9: Load-time data for a Low PVA gel.

Electroforce 5500.

There are a number of reasons theorized, such as the conditions of the freezer, the purity and molecular weight of the PVA M_w 31,000 - 50,000. The effect of the molecular weight of the PAA has also not been investigated and needs to be addressed to ensure that the gel used in the final composite is as close to the stiffness value of articular cartilage as possible.

4.2.5 Conclusions

The gels made exhibited a stiffness on the order of the 10 kPa range. This is still two orders of magnitude away from the 1-2 MPa range seen by articular cartilage. Improvements need to be made in order to make up this difference. By increasing the molecular weight of the

PVA in the gel, the stiffness also increases [31]. This will be used in a future gel to also allow for fracture testing of the PVA-PAA gel as the gels fabricated in this study were unable to be used for fracture testing.

4.3 High Molecular Weight PVA Hydrogels

4.3.1 Introduction

With the previous PVA-PAA gels falling short of the reported values in Offedu et al, the need to use a similar gel was necessary. The initial work on the PVA-PAA gels was conducted by the Peppas group in a series of papers describing how the gels were made [31]. Other papers have also concluded that the stiffness of the gel can be increased by using a higher molecular weight type of PVA. This updated gel will be made from PVA (M_w 85,000 - 124,000) in an attempt to increase the stiffness to a value closer to that of articular cartilage. The PVA was kept the same from the previous work as the PAA has been theorized to not have a significant impact on the stiffness [5, 30, 31]. By changing the base of the gel to a higher molecular weight, the stability and stiffness is increased to a point that produces a gel with properties much closer to that of biological tissues.

4.3.2 Methods

To start, 15% wt. solutions of PVA (M_w 85,000 - 124,000) (Sigma-Aldrich MO, USA), PAA (M_w~250,000), and PAA (M_w~450,000) were prepared by submersing the solutions in a 90 °C water bath and allowed to cool to room temperature. To form the gels, the PVA and one of the PAA solutions were mixed in a weight ratio of 3:1 and placed in an 85 °C water bath to ensure complete solvency of the solution. The PVA-PAA gel mixtures were then put into 35 mm petri dishes, Parafilm wrapped overtop, and allowed to sit for overnight, or at least 8 hours, to allow the air bubbles in the solutions to remove themselves. The gels were then placed in a -20 °C freezer for 23 hours and then thawed at room temperature, 23 °C for an hour. The gels underwent 8 cycles. 10 samples from each of the two groups were taken for testing before swelling, 8 for fracture and two for indentation. The second set of gels were placed in an excess, at least 150% of the weight of the gel, of a 0.1 M sodium hydroxide

solution for 48 hours until equilibrium. After swelling, the gels were washed with water to ensure safety before testing. For the fracture tests, the methods used in chapter 3.4 and 4.2
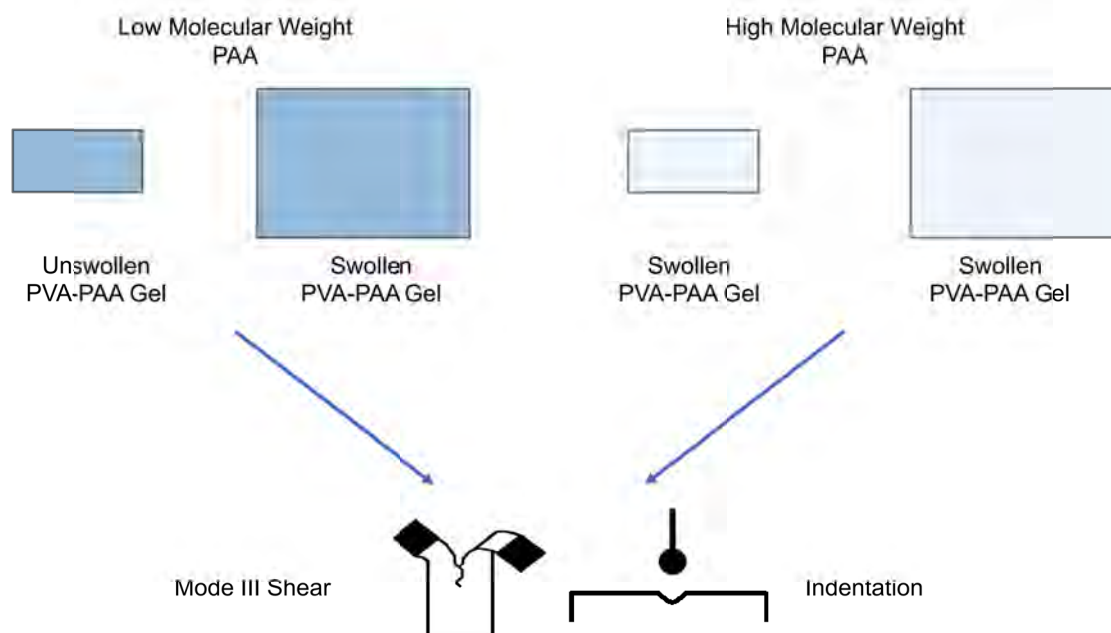
Figure 4.10: Experimental design for testing the gel portion of the composite. The four test groups are designed to investigate the contributions that the molecular weight of PAA has on the gel.

were adapted and used with the gels, a slightly larger cut, 7.5 mm versus the 5 mm used for the paper and electrospun fibers was used to allow for better attachment of the gel to the metal grips. A total of eight samples for each of the two groups were tested.

Indentation was used with a 7 mm indenter probe and a indentation depth of 1 mm. The hold time was set at 300 seconds and a ramp time of 5 seconds was used. Each individual gel was tested four separate times in different locations to prevent the effects of previous tests impacting the measurements. Two gels were used for each group and tested a total of four times each.

4.3.3   Results

The different molecular weight PAA had an impact on the swelling of the gels. The increasing molecular weight lead to an increase in the diameter of the gels. In the swollen state the diameter increased from an average of 43.2 ± 0.8 mm in the low molecular weight group to

53

47.0 ± 1.3 mm in the high molecular weight group. The thickness of the gels also changed with an average value of 4.0 ± 0.4 mm and 4.8 ± 0.4 mm for the swollen gels. The unswollen state of the gels the diameter for the low PAA group was 32.7 ± 0.5 mm and their thickness was 3.6 ± 0.5 mm. The unswollen high PAA group had diameter and thickness values of 33.6 ± 0.2 mm and 3.0 ± 0.4 mm respectively. Mode III shear testing revealed the fracture
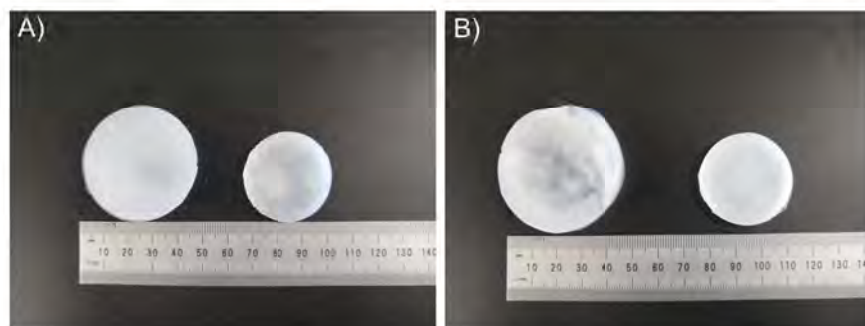
Figure 4.11: Comparisons for the swollen and unswollen states for the PVA-PAA gels. (A) shows the low PAA (M_w ˜250,000) gel and (B) shows the high PAA (M_w ˜450,000).

toughness of the gels. Shown by Figure 4.12, the unswollen groups performed better when compared to their swollen counterparts, however, the high PAA group outperformed the low PAA group. The unswollen, low PAA gels reported a fracture toughness of 335 ± 55 Jm^{-2}
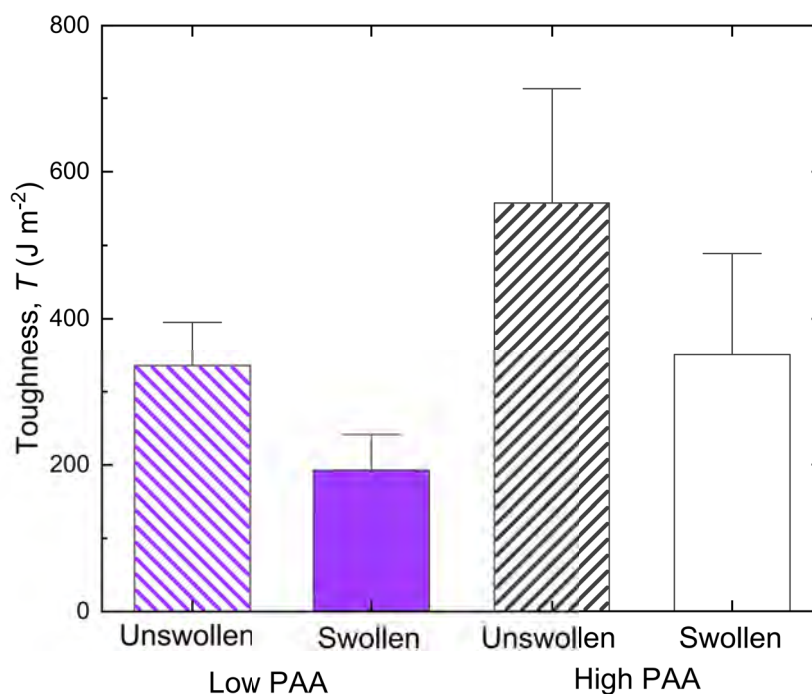
Figure 4.12: Mode III fracture data for the PVA-PAA gels.

compared to the 192 ± 45 Jm^{-2} exhibited by the swollen, low PAA gels. The high PAA gels reported 557 ± 145 Jm^{-2} and 350 ± 129 Jm^{-2} for the unswollen and swollen groups respectively.

Indentation testing and the subsequent viscoelastic and poroelastic analysis allowed for the calculation of the shear modulus, viscoelastic ratio, the pore size, and Poisson's ratio for the gels. The viscoelastic results for the gels are shown in Figure 4.13. The voscoelastic ratio for
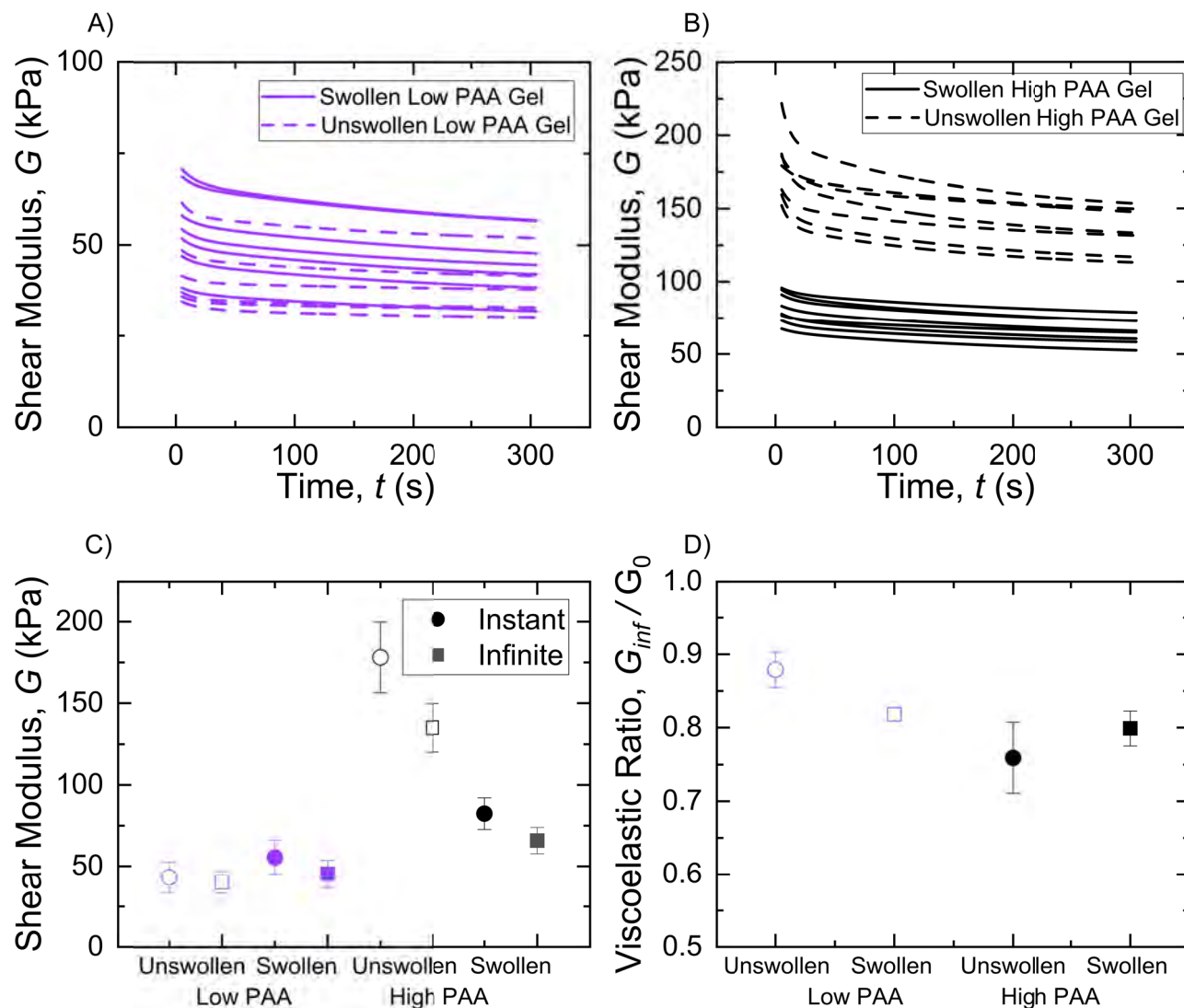
Figure 4.13: Composite figure showing the results of the viscoelastic analysis for the PVA-PAA gels. (A) Shows the modulus over time for the low PAA gels. (B) Shows the modulus over time for the high PAA gels. (C) The instantaneous and infinite shear modulii for all of the gels (D) The viscoelastic ratio of the gels.

each of the gels are 0.87 ± 0.02 and 0.81 ± 0.009 for the unswollen and swollen low PAA gels respectively. The viscoelastic ratio decreased slightly from to low PAA group to the high

PAA group. The unswollen and swollen high PAA gels had a viscoelastic ratio of 0.75 ± 0.05 and 0.79 ± 0.02 respectively. The viscoelastic analysis provided instantaneous, $t = 0$, and
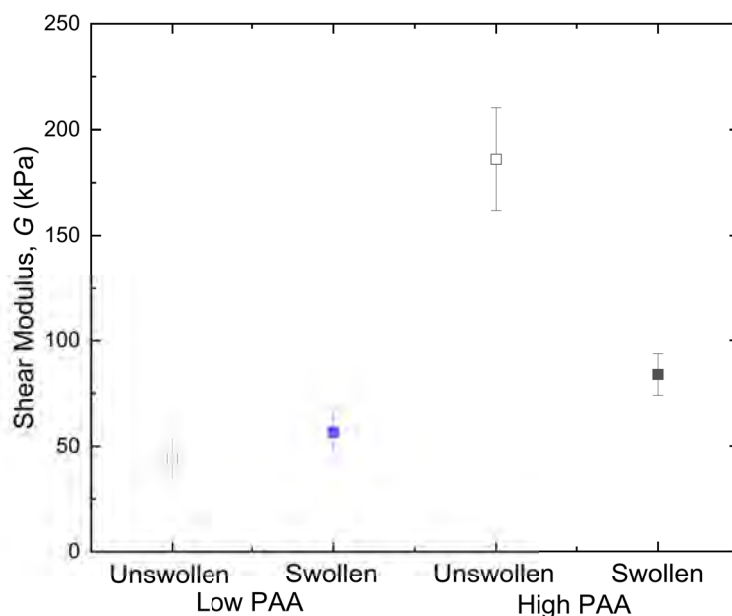
Figure 4.14: Shear modulus taken from the poroelastic analysis of the gels.

infinite, $t = 300$, shear modulus values. The instantaneous values for the shear modulus are 43.2 ± 9.4 kPa and 55.6 ± 10.6 kPa for the unswollen and swollen low PAA gels and 178.2 ± 21.7 kPa and 82.4 ± 9.7 kPa for the unswollen and swollen high PAA group. The infinite shear modulus values are 40.2 ± 6.7 kPa and 45.5 ± 8.4 kPa for the unswollen and swollen low PAA group. The high PAA group performed better with an infinite shear modulus of 134.9 ± 14.8 and 65.8 ± 8.1 kPa.

The poroelastic data proved to provide a close match to the viscoelastic analysis. The shear modulus for the low PAA gels was 44.2 ± 9.9 kPa and 56.5 ± 10.8 kPa for the unswollen and swollen gels. The unswollen and swollen high PAA gels had a shear modulus of 186.1 ± 24.2 kPa and 83.8 ± 9.9 kPa.

4.3.4 Discussion

An unexpected result was the impact of the molecular weight of the PAA on the material. The PAA from previous articles was seen mostly as a vector to allow for the introduction of

Table 5: High PVA Gel Poroelastic Data

Gel Type	Shear Modulus, G (kPa)	Permeability, κ (cm^2)	Poisson's Ratio. ν
Low PAA Unswollen	44.2 ± 9.9	1.58E -14 ± 2.98E -14	0.42 ± 0.019
Low PAA Swollen	56.5 ± 10.8	1.05E -13 ± 1.88E -14	0.38 ± 0.009
High PAA Unswollen	186.1 ± 24.2	7.44E -14 ± 1.7E -14	0.31 ± 0.05
High PAA Swollen	83.3 ± 9.9	7.67E -14 ± 1.42E -14	0.36 ± 0.02

hydroxide ions after swelling [32]. The data seen in this study suggests that the inclusion of PAA is significant for more than just the addition of charged ions into the structure. The change of the structure of the gel from the unswollen to the swollen state can be one of the reasons for the increase in the stiffness between the high PAA and Low PAA. As can be
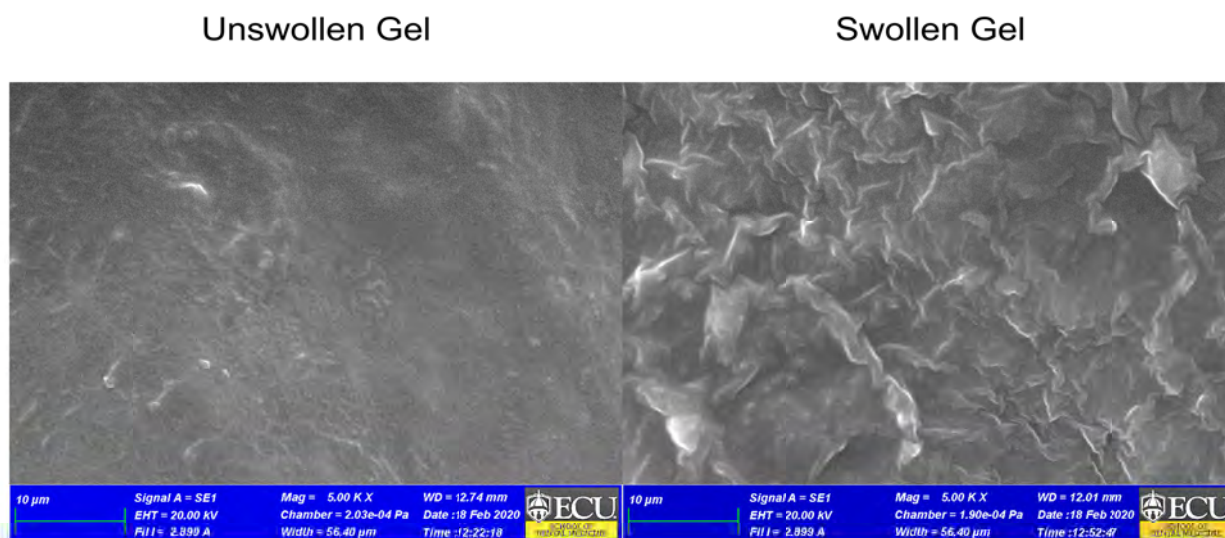
Figure 4.15: SEM image of both the swollen and unswollen gel. The gels were freeze-dried prior to imaging.

seen in Figure 4.14, the change in the surface topography shows that the swollen state has changed the arrangement of the polymer chains. This change in the polymer chain arrangement is possible due to the physical bond formed between the chains of molecules. This suggests that the polymer chains are effected by not only the presence of ions in the matrix, but the length of the molecule involved in the matrix also plays an important role in how

the gel behaves. This is also seen in the fracture data as the high molecular weight gel was more tough than the low molecular weight counter part.

The impact of using both viscoelastic and poroelastic analysis can be seen as both of the analysis provided similar shear modulus results. This is not surprising as both of the analysis are derived form relations with basic elasticity. Both of the analysis providing similar answers provides a level of confidence with the results of the tests. This level of confidence is also important because of the planned construction of the composite materials. The composites will be fabricated using a single layer of the electrospun fibers which is at most 0.5 mm thick. This thickness is not conducive to macroscale indentation and other methods of investigating the stiffness of the material will be used.

The change from the low molecular weight PVA (M_w31,000-50,000) to the high molecular weight PVA (M_w85,000-124,000) did increase the stiffness of the gels substantially from around 6,000 kPa for the low PVA gels to around 175 kPa for the best performing high PVA gel. A change on of about two orders of magnitude which brings the stiffness values much closer to the MPa values recorded for articular cartilage.

4.3.5   Conclusions

The change from low PVA to high PVA proved to be effective as the stiffness of the gels improved to the 100 kPa range. This increase is much closer to the 1 MPa range seen in articular cartilage. The gels were also able to successfully undergo fracture testing due to the gels being much more robust that the low PVA counterparts. Both modes of testing, indentation and fracture, gave valuable insight into the stiffness and strength of the gel and the importance of the molecular weight of the PAA on the mechanical properties of the gel. With the importance of the molecular weight of the PAA in mind, the gel high PVA-high PAA gel was chosen to be the gel component of the composite as it exhibted improved stiffness and toughness over the high PVA-low PAA gel.

5 The Hydrogel-Nanofiber Composite

5.1 Introduction

After changing the gel to use higher molecular weight polymer, a composite material with the inclusion of the hydrogel, gelatin fibers, and charged ions was ready. Based on the gel study, it was decided to use the high molecular weight PVA (M_w86,000 - 124,000)and high molecular weight PAA (M_w~450,000). This as decided due to the stiffness of the gel being the highest.

5.2 Methods

Two types of fibers were made for use in the composites, crosslinked and uncrosslinked. These were made using the methods described in section 3.4. These fibers were fabricated and allowed to dry in a dessicator. The fibers were cut into 1.3 in (33 mm) diameter circles for use in the composites. For the composites, a single layer of fibers was used to simplify fabrication.

Once the fibers were cut and ready for use, the 15% wt. PVA and PAA solutions were mixed in a 3:1 by weight ratio of PVA and PAA respectively accroding to methods described in section 4.3. A thin layer of gel was placed on the bottom of a petri dish and smeared to allow for the distribution of a thin layer due to the high viscosity of the solution. A single fiber mat as placed on the layer of gel and then manipulated with tweezers to ensure the fiber mat did not fold in on itself. The composites were then allowed to sit at room temperature for 24 hours to eliminate air bubbles caused by the procedure. Fourty-four composites were made in total split among four different groups, with 10 used for testing and the last four used as a reserve for each group. There were two over arching groups of composites with the type of electrospun fiber mat used in the composite with one group using uncrosslinked composites and the other using crosslinked composites. The two groups were then split in half with 10 being placed in a 0.1 M sodium hydroxide solution for swelling and 10 tested as fabricated in an unswollen state. The fiber mat and gel composite was then crosslinked by
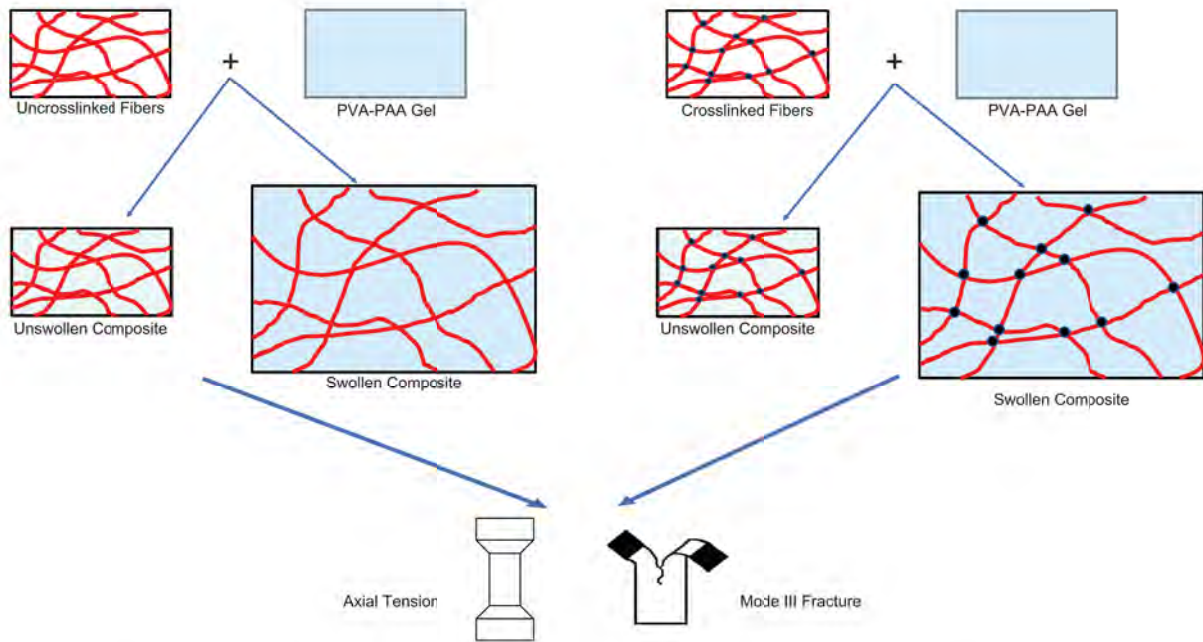
Figure 5.1: Experimental design for testing the composite materials. With four different test groups and two forms of mechanical testing, mode III fracture and axial tension.

repeated freeze-thaw cycles. The composites were subjected to eight cycles, with a 23 hour freeze followed by a 1 hour thaw.

Fracture testing of the composites was performed in mode III shear similar to the paper and gels tested in earlier sections. Due to the smaller size of the composites, the dimensions of the cut and tear distance were changed to a cut size of 10 mm and a tear distance of 7.5 mm. This testing took a total of 20 seconds to complete. Six samples from each of the four groups were tested and the fracture toughness of the samples analyzed from the thickness of the sample and the average force seen during tearing.

Tensile testing was performed on the Electroforce 5500 and 25 N load cell with metal grips. The samples were cut into 25 mm x 10 mm rectangles for testing using a guide. As some samples were not quite 25 mm in diameter, they were cut into a rectangle and measured using a ruler to determine the length of the sample. All samples had gauge marks placed on them to ensure that the grips were in the proper location for testing. The samples were tested at 0.5 mm/s to a total displacement of 10 mm. Four samples from each of the four

groups were tested and the load-time data analyzed to obtain the elastic modulus from the linear portion of the data, the ultimate tensile strength, the strain energy density, and the stress at failure.

5.3   Results

The composites after fabrication had noticeable differences depending on the swelling. Composites that underwent swelling were more translucent than the unswollen composites which were more opaque and had a white color from the gel and the fibers inside of the matrix. The swollen composites also had a glossy appearance while the unswollen composites were matte in appearance. The size of the composite also depended on the type of fiber used in
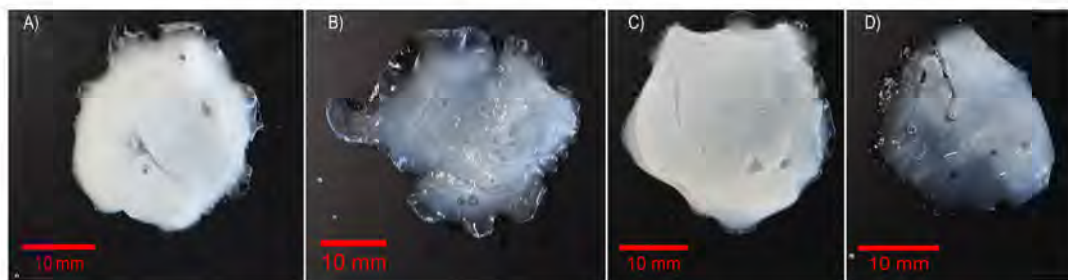
Figure 5.2: (A) An unswollen, uncrosslinked composite after fabrication. (B) A swollen, uncrosslinked composite after fabrication. (C) Crosslinked unswollen composite. (D) Crosslinked swollen composite.

the composite and the condition of the gel. The uncrosslinked composites were smaller than the crosslinked composites with 20.4 ± 2.1 mm and 24.2 ± 1.9 mm for the diameter of the unswollen and swollen uncrosslinked composites. The crosslinked composites had a diameter of 25.7 ± 3.1 mm and 30.1 ± 4.5 mm for the unswollen and swollen composites respectively.

The thickness of the composites largely depended on the gel portion of the composite as the gel is a viscous liquid before crosslinking. The thickness of the uncrosslinked gels were slightly larger at 1.4 ± 0.4 mm and 1.1 ± 0.3 for the unswollen and swollen conditions. The crosslinked composites were easier to manipulate during fabrication due to the water resistance gained by the addition of the crosslinkers to the gelatin. Even without fluorescence, the fiber mats can be seen with the naked eye, having been unaffected by either the crosslinking or swelling of the gel component. There were air bubbles present on some of the composites.

The cuts made in the fracture tests were made to minimize the effect of those defects from impacting the test. The data gathered from the fracture tests shows the unswollen groups
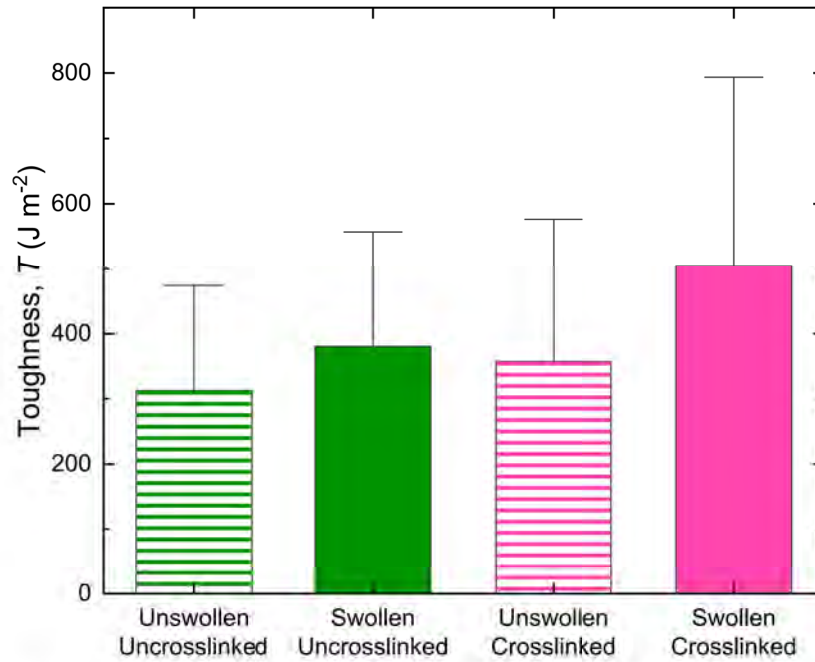
Figure 5.3: Graph of the toughness for each of the four test groups.

performing worse than the swollen groups with $312 \pm 147\ Jm^{-2}$ and $358 \pm 195\ Jm^{-2}$ for the uncrosslinked and crosslinked composites. The swollen composites improved with $328 \pm 184\ Jm^{-2}$ and $420 \pm 280\ Jm^{-2}$ for the uncrosslinked and crosslinked swollen composites respectively. Following the tensile tests, the composites had different forms of failure. Some
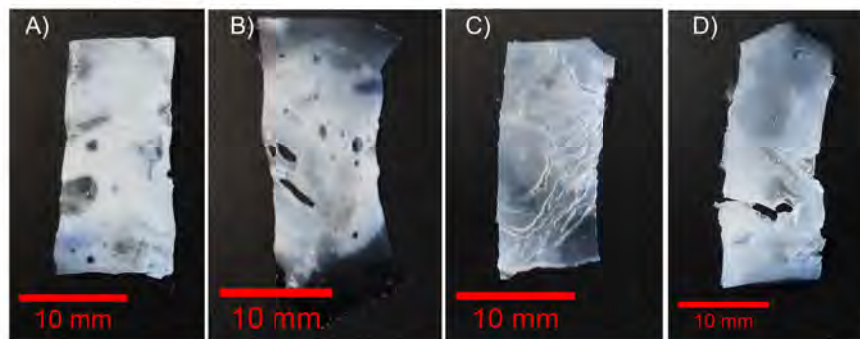
Figure 5.4: (A) Uncrosslinked, unswollen composite that underwent tensile testing but did not fail due to the high compliance of the sample. (B) Uncrosslinked, unswollen composite that underwent tensile testing and shows evidence of void coalescence. (C) Uncrosslinked, swollen sample that has many small cracks develop in the matrix due to tensile testing. (D) Uncrosslinked, swollen composite that has a failure develop in the lower half of the sample stop due to the presence of fibers in the matrix.

of the samples did not fail due to the high compliance of the material combined with the 10 mm range of the test. An example of such a composite can be seen in Figure 5.4 (A). The scaffold in Figure 5.4 (B) did have signs of void coalescence as defects formed in the composite but did not cause the material to fail. This is in contrast to the visible air pockets
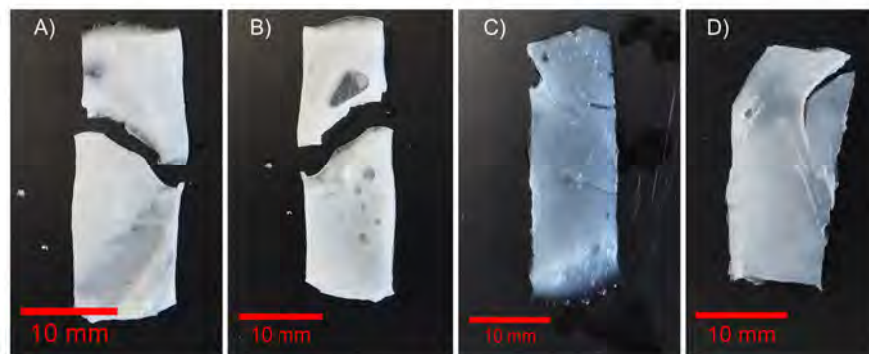
Figure 5.5: (A) The front side of a crosslinked, unswollen composite that has failed during the tensile test. (B) The reverse side of the same composite in A). (C) A crosslinked, swollen composite that has failure cracks showing on the right side of the material. (D) This crosslinked swollen composite had a crack develop and deflect due to the presence of the electrospun fibers in the matrix.

in the scaffold from fabrication. The voids did not start in the location of the air pockets. Composite (C) in Figure 5.4, had small cracks form on the right hand side of the composite.

Figure 5.5 shows crosslinked composites after testing. Parts (A) and (B) show the same composite and crack deflection can be observed as the crack first propagated perpendicular to the load but then was deflected by the presence of fibers in the matrix. This same deflection can be seen in (D) with a crack forming near the top of the composite and deflecting almost back in on itself. The elastic modulus for the composite scaffolds is reported at 32.2 ± 17.7 kPa for the uncrosslinked unswollen composites, 35.8 ± 15.8 kPa for the uncrosslinked swollen composites, 28.9 ± 14.1 kPa for the crosslinked unswollen and 27.8 ± 6.9 kPa.

5.4   Discussion

The composites made here show improvement over just the individual components. The toughness of the composites is better than that of the bulk gel. The elastic modulus is much smaller than that of the gel by an order of magnitude. The decrease in the stiffness of the gels can be attributed to the extremely high compliance of the composite experiencing strains
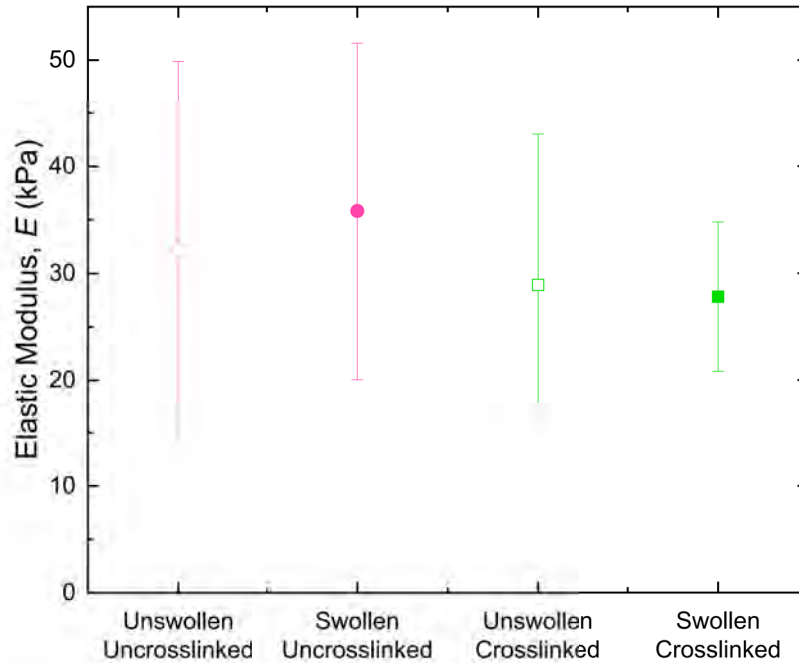
Figure 5.6: Graph of the elastic modulus from the tensile testing of the composites.

upwards of 20% and 30% before the limits of the mechanical testing machine is reached. This also does not take into account any of the strain-rate dependent effects of the material. The strain rate of 0.5 mm/s is small and if the test was repeated at a faster strain rate, a different elastic modulus would be observed as a change in the slope of the load-time curve. Another impact of the difference in testing was the direction of the load. In indention, the load applied to the material is compressive and interacts in a stiffening manner with the charged ions in the gel matrix. In tension, the charged ions are unable to interact, greatly decreasing the stiffness of the gel or composite being tested. Another important note is the difficulty in working with biological like materials is maintaining proper gripping of the material during testing. This was slightly alleviated by the addition of sandpaper-like grit added to the metallic grips. However, future testing using methods such as indentation that do not rely on the presence of grips is suggested.

The fracture results are much more promising, showing an improvement in the toughness of the material due to the inclusion of the electrospun fibers to the gel. The values for the toughness are only about half of the values seen in cartilage [3].
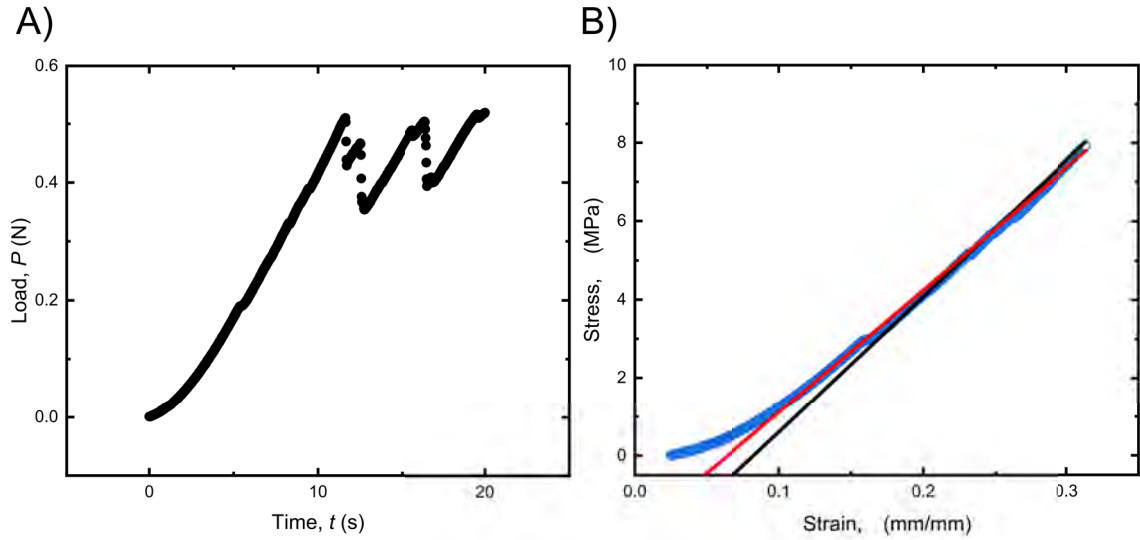
Figure 5.7: (A) Example load-time graph for the tensile testing of a composite. (B) Section of the graph taken and analyzed with lines to estimate the elastic modulus from the slope of the graph.

5.5   Conclusions

Fracture testing and tensile testing of the composites provided the toughness and stiffness of the composite material. The main limitation with the estimation of the stiffness is that the mode of testing placed the material in tension, not the compression that would normally be seen in a material used for the replacement of articular cartilage. The composite improved its toughness when compared to the gel bringing it closer in line with values seen in articular cartilage.

6   Conclusions and Future Directions

In this study, various materials were investigated for use in a biomimetic composite to replace and replicate the function of articular cartilage. The two materials investigated were hydrogels and electrospun fiber mats. These two materials, hydrogels and electrospun fibers, serve to replicate a specific portion of cartilage, with the hydrogel providing water and the charged ions while the electrospun fibers are added to reinforce the structure and mimic the presence of collagen fibers in cartilage. Characterization of the materials was undertaken using the mechanical models of elasticity and viscoelasticity and the structural model of poroelasticity. The materials focused in here were hydrogels, a class of material with a high water content that has seen extensive use in tissue engineering applications due to its biocompatability. Simple agar hydrogels and sodium polyacrylate gels helped understand the basic functions of swelling and time dependent behavior. Time dependent behavior is important and general elasticity does not have the capability to handle the calculations necessary with time-dependent functions.

Viscoelasticity and poroelasticity are methods to expand elasticity to handle time-dependent functions by modeling either the behavior or the underlying structure of the material being investigated. After modeling the behavior of simple hydrogels and developing methods to test the different components of the composite, the electrospun fibers and gels were tested independently before inclusion into the composite. Figure 6.1 summarizes the methods for the creation and testing of the composites and its components. More complex PVA-PAA hydrogels with charged ions were investigated to increase the stiffness of current hydrogels by the interaction of charged ions when in close proximity to one another. By adjusting the molecular weight of either component in the PVA-PAA poly electrolyte hydrogel, changes were observed in the stiffness from indentation testing and viscoelastic and poroelastic analysis. An increase in the toughness of the material was observed after performing mode III shear tests on the gels. The benefit of performing mode III over other forms of fracture testing is that the energy used to deform the material is minimized which is crucial when testing materials with high compliance. After testing and characterizing the gel the other
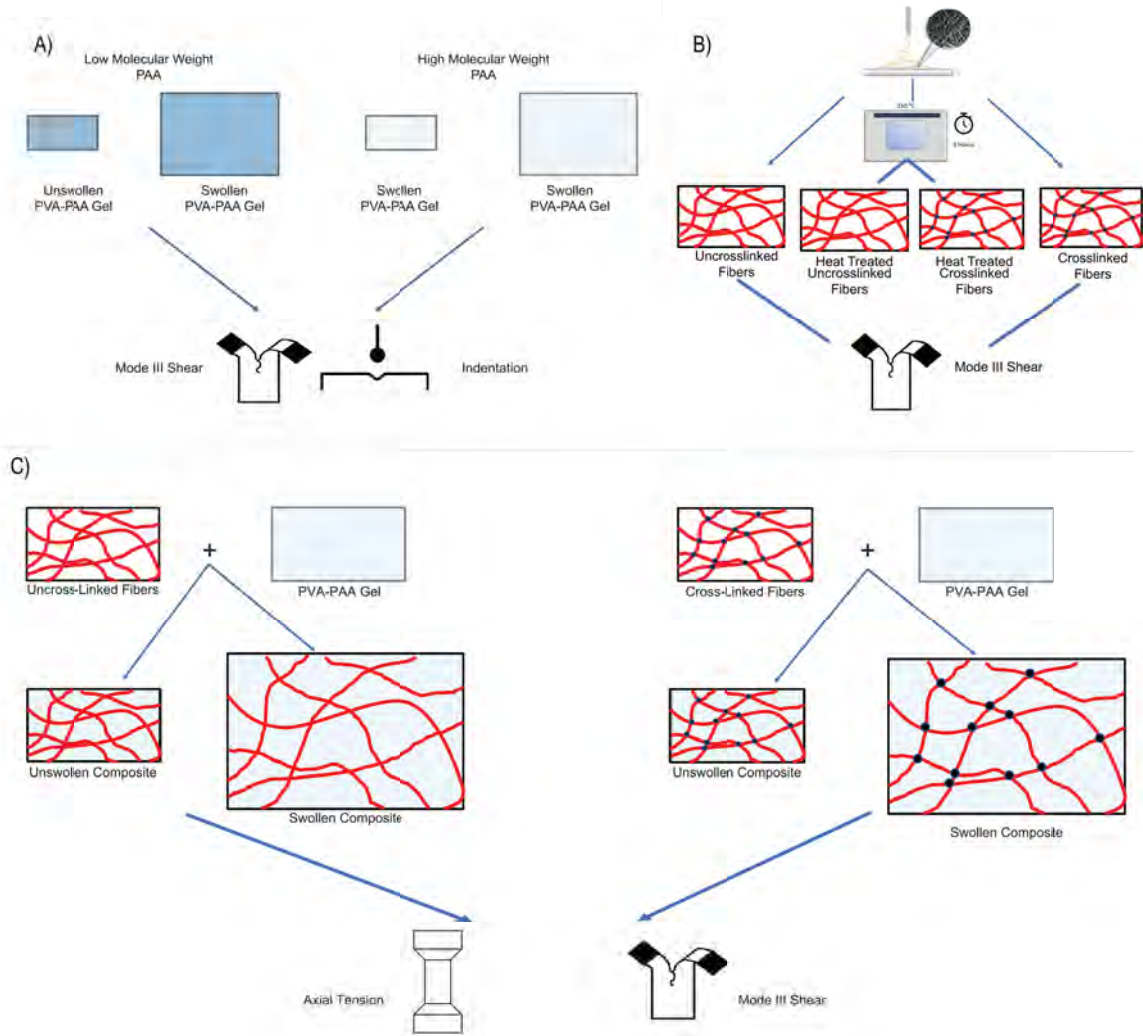
Figure 6.1: (A) The different test groups and testing methods used for the investigation into PVA-PAA hydrogel. (B) The test groups investigated for the electrospun fibers. (C) By combining the electrospun fibers and gel, a composite material was made and tested.

component of the composite, electrospun fibers, were also investigated with differences in crosslinking and heat treatment. With the addition of crosslinkers and heat treatment, the electrospun scaffolds showed an increase in the toughness of the material. The crosslinkers also applied a level of water stability to the scaffolds that improved the later fabrication of the composites. There are four important results that are worth mentioning. Investigation into the electrospun fibers saw the large impact that heat treatment had on the electrospun
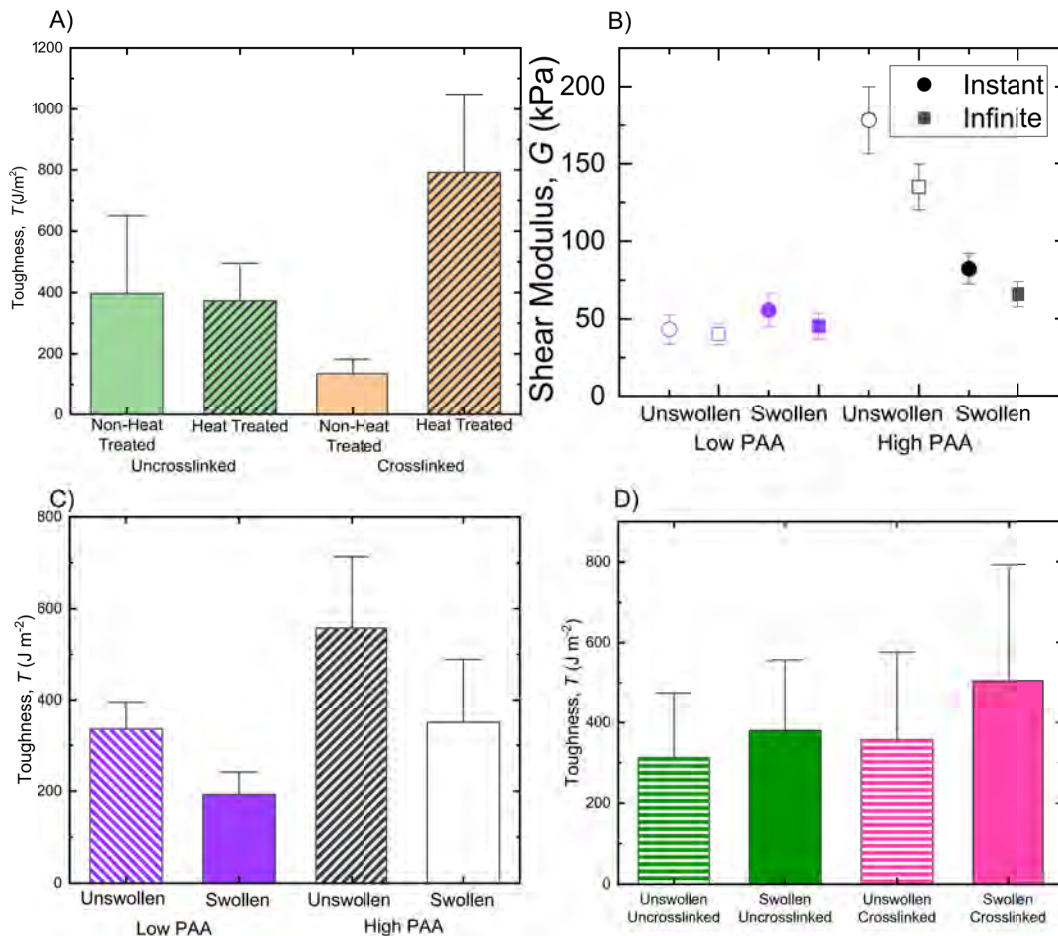
Figure 6.2: (A) The fracture toughness of the electrospun fibers, noteably the increase in toughness for the heat treatment of the crosslinked fibers. (B) The shear modulus values, both instant and infinite, for the High-PVA gels. An increase in stiffness by changing the molecular weight of the PAA was observed. (C) The toughness of the PVA gels with an increase in toughness associated with an increase in the molecular weight of the PAA used. (D) Toughness of the composite material seeing an increase with both swelling and crosslinking. Also showing an improvement over the comparable gel component.

fibers with crosslinkers. The increase from a value of $135 \pm 44\ Jm^{-2}$ to $791 \pm 242\ Jm^{-2}$, a nearly 6 fold increase in the toughness of the material. The impact of the molecular weight of the PAA used on the material stiffness was an interesting result as this has not been investigated before and allows for the fine tuning of mechanical properties for different purposes in the future. The increase in toughness also seen indicates that there are complex chain interactions between the PVA and PAA molecules as generally, an increase in stiffness comes at the cost of material toughness. Part (C) of Figure 6.2 shows this increase in toughness seen in the high PAA gels when compared to the low PAA gels. The final noteworthy result is the increase in toughness seen in the composites with both crosslinking and swelling

of the composites. Further testing is needed to identify the complex interactions between the charged ions, hydrogel, and gelatin fibers. The reason why the tensile data from the composites is not shown here is because of the discrepancy between placing a material in compression and placing a material in tension.

Cartilage is a material that is highly anisotropic and when testing cartilage in bulk the results are dependent on the orientation of the section of cartilage and where the cartilage sample is taken from [3]. For human articular cartilage, an average value of the shear modulus is 0.23 MPa [3]. The values of 83.8 kPa obtained in this paper for the indentation shear modulus converts to 0.0838 MPa for the swollen composite. Interestingly, the unswollen composite has a shear modulus value of 0.186 MPa and is much closer to the shear modulus of cartilage. As the gel makes up the majority of the composite by weight and volume, it is reasonable to assume that the shear modulus of the composites is close to the values reported by the gels. The Poisson's ratio of cartilage is also highly dependent on the orientation and method of testing, for indentation testing, Poisson's ratio tends to reach values around 0.4 [3,33]. The values of the low PAA gels were the closest to this with 0.42 and 0.38.

Improvements that could be made to the composite would be to swap the gelatin for collagen. Gelatin contains small amounts of collagen. With collagen being the main contributer to the tensile strength of cartilage this change would hopefully increase the stiffness and toughness of the material further. Also, making sure to properly include 10 - 15 % collagen into the material. This was limited by the thickness of the electrospun fiber mats in the composite fabrication and presents another engineering challenge for the future to produce electrospun mats multiple millimeters thick. Because of the physics of electrospinning, the longer the electrospinning continues, an insulating layer is deposited on the collecting surface reducing the affinity for the deposition of new fibers. Layering multiple mats onto the surface is possible but previous issues with lamination of fiber reinforced gels limited the layers to only a single one in this study [16]. Increasing the total thickness of the composite also would allow for reliable indentation of the composite material giving another lens to view the material properties from. Reliable indentation is important because of the difficulty in the acquisition

of data from tensile tests due to the problem of gripping the samples in their saturated state.

Many soft tissues such as cartilage are difficult to work with traditional engineering characterization techniques such as tensile testing. Other techniques such as microscopic magnetic resonance elastography are developed to non-destructively characterize soft tissues [34]. Other possible methods of investigating the stiffness include ultrasound shear wave elastography. These two methods provide a different lens to view the material from, but use frequencies in sound and in dynamic loading that are much higher than normal and run into the same difficulties with sample thickness that indentation has. With a thinner sample higher frequencies must be used to decrease the size of the wave and characterize the tissue.

Even with the characterization shown in this thesis, and the work described with dynamic testing, two areas that were not covered in this study that would need to be addressed before this material could be considered as a possible replacement for articular cartilage. Friction is a large component of the wear that eventually causes osteoarthritis, investigation of the frictional component of this material is critical. The choice to focus on the stiffness and toughness was to make a material that was robust enough to withstand the biomechanical forces so that the material would not fail due to normal locomotion.

Another area that was considered for inclusion into this study was biocompatability. Live-dead assays and investigating the proteins and products of stem cells seeded on these scaffolds would tell how the cells respond to the mechanical environment around them and allow researchers to make adjustments to the material based on how the cells react. The creation of tissue is a complex process and without investigating how cells react to the environment, researchers only have a general direction in the area of needed progress.

With the fabrication of this hydrogel-nanofiber composite, the field of biomimicry continues to be a promising source of inspiration for new ideas and techniques for creating materials that simulate the behavior of biological tissues and even creates the possibility of robust

materials for non-biological applications.

References

[1] D. G. Strange, "Mechanics of Biomimetic Materials for Tissue Engineering of the Intervertebral Disc," PhD, University of Cambridge, 2012.

[2] L. B. Murphy, M. G. Cisternas, D. J. Pasta, C. G. Helmick, and E. H. Yelin, "Medical Expenditures and Earnings Losses Among US Adults With Arthritis in 2013," *Arthritis Care and Research*, vol. 70, no. 6, pp. 869–876, 2018.

[3] V. C. Mow, W. Y. Gu, and F. H. Chen, "Structure and Function of Articular Cartilage and Mensicus," *Basic Orthopaedic Biomechanics and Mechano-Biology*, 2005.

[4] G. Filardo, E. Kon, A. Roffi, A. Di Martino, and M. Marcacci, "Scaffold-based repair for cartilage healing: A systematic review and technical note," *Arthroscopy - Journal of Arthroscopic and Related Surgery*, vol. 29, no. 1, pp. 174–186, 2013.

[5] G. S. Offeddu, I. Mela, P. Jeggle, R. M. Henderson, S. K. Smoukov, and M. L. Oyen, "Cartilage-like electrostatic stiffening of responsive cryogel scaffolds," *Scientific Reports*, vol. 7, no. October 2016, pp. 1–10, 2017. [Online]. Available: http://dx.doi.org/10.1038/srep42948

[6] S. Jahn, J. Seror, and J. Klein, "Lubrication of Articular Cartilage," *Annual Review of Biomedical Engineering*, vol. 18, no. 1, pp. 235–258, 2016. [Online]. Available: http://www.annualreviews.org/doi/10.1146/annurev-bioeng-081514-123305

[7] C. B. Carballo, Y. Nakagawa, I. Sekiya, and S. A. Rodeo, "Basic Science of Articular Cartilage," *Clinics in Sports Medicine*, vol. 36, no. 3, pp. 413–425, 2017.

[8] D. Goyal, S. Keyhani, E. H. Lee, and J. H. P. Hui, "Evidence-based status of microfracture technique: A systematic review of Level I and II studies," *Arthroscopy - Journal of Arthroscopic and Related Surgery*, vol. 29, no. 9, pp. 1579–1588, 2013. [Online]. Available: http://dx.doi.org/10.1016/j.arthro.2013.05.027

[9] K. Mithoefer, T. Mcadams, R. J. Williams, P. C. Kreuz, and B. R. Mandelbaum, "Clinical efficacy of the microfracture technique for articular cartilage repair in the

knee: An evidence-based systematic analysis," *American Journal of Sports Medicine*, vol. 37, no. 10, pp. 2053–2063, 2009.

[10] J. D. Harris, R. A. Siston, X. Pan, and D. C. Flanigan, "Autologous chondrocyte implantation: A systematic review," *Journal of Bone and Joint Surgery - Series A*, vol. 92, no. 12, pp. 2220–2233, 2010.

[11] G. Bentley, L. C. Biant, S. Vijayan, S. Macmull, J. A. Skinner, and R. W. J. Carrington, " Minimum ten-year results of a prospective randomised study of autologous chondrocyte implantation versus mosaicplasty for symptomatic articular cartilage lesions of the knee ," *The Journal of Bone and Joint Surgery. British volume*, vol. 94-B, no. 4, pp. 504–509, 2012.

[12] Q. H. Zhang, A. Cossey, and J. Tong, "Stress shielding in periprosthetic bone following a total knee replacement: Effects of implant material, design and alignment," *Medical Engineering and Physics*, vol. 38, no. 12, pp. 1481–1488, 2016. [Online]. Available: http://dx.doi.org/10.1016/j.medengphy.2016.09.018

[13] H. Kamata, X. Li, U. I. Chung, and T. Sakai, "Design of Hydrogels for Biomedical Applications," *Advanced Healthcare Materials*, vol. 4, no. 16, pp. 2360–2374, 2015.

[14] A. C. Chen, S. Varghese, Y. Hwang, R. L. Sah, and Q. T. Nguyen, "Cartilage-like mechanical properties of poly (ethylene glycol)-diacrylate hydrogels," *Biomaterials*, vol. 33, no. 28, pp. 6682–6690, 2012.

[15] F. Anjum, A. Carroll, S. A. Young, L. E. Flynn, and B. G. Amsden, "Tough, Semisynthetic Hydrogels for Adipose Derived Stem Cell Delivery for Chondral Defect Repair," *Macromolecular Bioscience*, vol. 17, no. 5, pp. 1–13, 2017.

[16] K. Tonsomboon, A. L. Butcher, and M. L. Oyen, "Strong and tough nanofibrous hydrogel composites based on biomimetic principles," *Materials Science and Engineering C*, vol. 72, pp. 220–227, 2017. [Online]. Available: http://dx.doi.org/10.1016/j.msec.2016.11.025

[17] V. S. Chernonosova, A. A. Gostev, Y. Gao, Y. A. Chesalov, A. V. Shutov, E. A. Pokushalov, A. A. Karpenko, and P. P. Laktionov, "Mechanical properties and biological behavior of 3D matrices produced by electrospinning from protein-enriched polyurethane," *BioMed Research International*, vol. 2018, 2018.

[18] Z. Guo, J. Xu, S. Ding, H. Li, C. Zhou, and L. Li, "In vitro evaluation of random and aligned polycaprolactone/gelatin fibers via electrospinning for bone tissue engineering," *Journal of Biomaterials Science, Polymer Edition*, vol. 26, no. 15, pp. 989–1001, 2015.

[19] N. Zhu and X. Che, "Biofabrication of Tissue Scaffolds," *Advances in Biomaterials Science and Biomedical Applications*, 2013. [Online]. Available: http://www.intechopen.com/books/advances-in-biomaterials-science-and-biomedical-applications/biofabrication-of-tissue-scaffolds

[20] K. Tonsomboon, D. G. Strange, and M. L. Oyen, "Gelatin nanofiber-reinforced alginate gel scaffolds for corneal tissue engineering," *Proceedings of the Annual International Conference of the IEEE Engineering in Medicine and Biology Society, EMBS*, pp. 6671–6674, 2013.

[21] K. Siimon, H. Siimon, and M. Järvekülg, "Mechanical characterization of electrospun gelatin scaffolds cross-linked by glucose," *Journal of Materials Science: Materials in Medicine*, vol. 26, no. 1, pp. 1–9, 2015.

[22] T. Vieira, J. C. Silva, J. P. Borges, and C. Henriques, "Synthesis, electrospinning and in vitro test of a new biodegradable gelatin-based poly(ester urethane urea) for soft tissue engineering," *European Polymer Journal*, vol. 103, no. April, pp. 271–281, 2018. [Online]. Available: https://doi.org/10.1016/j.eurpolymj.2018.04.005

[23] K. Tonsomboon and M. L. Oyen, "Composite electrospun gelatin fiber-alginate gel scaffolds for mechanically robust tissue engineered cornea," *Journal of the Mechanical Behavior of Biomedical Materials*, vol. 21, pp. 185–194, 2013.

[24] T. E. Brown, B. J. Carberry, B. T. Worrell, O. Y. Dudaryeva, M. K. McBride, C. N. Bowman, and K. S. Anseth, "Photopolymerized dy-

namic hydrogels with tunable viscoelastic properties through thioester exchange," *Biomaterials*, vol. 178, pp. 496–503, 2018. [Online]. Available: http://linkinghub.elsevier.com/retrieve/pii/S0142961218302394

[25] J. M. Mattice, A. G. Lau, M. L. Oyen, and R. W. Kent, "Spherical indentation load-relaxation of soft biological tissues," *Journal of Materials Research*, vol. 21, no. 8, pp. 2003–2010, 2006.

[26] L. P. Li and W. Herzog, "Strain-rate dependence of cartilage stiffness in unconfined compression: The role of fibril reinforcement versus tissue volume change in fluid pressurization," *Journal of Biomechanics*, vol. 37, no. 3, pp. 375–382, 2004.

[27] I. Garibi and S. Adams, "Making of Printer Paper," pp. 1–3, 2019. [Online]. Available: https://www.happyfolding.com/paper-making_of_printer_paper

[28] A. L. Butcher, C. T. Koh, and M. L. Oyen, "Systematic mechanical evaluation of electrospun gelatin meshes," *Journal of the Mechanical Behavior of Biomedical Materials*, vol. 69, no. February, pp. 412–419, 2017. [Online]. Available: http://dx.doi.org/10.1016/j.jmbbm.2017.02.007

[29] Q. Jiang, H. Xu, S. Cai, and Y. Yang, "Ultrafine fibrous gelatin scaffolds with deep cell infiltration mimicking 3D ECMs for soft tissue repair," *Journal of Materials Science: Materials in Medicine*, vol. 25, no. 7, pp. 1789–1800, 2014.

[30] C. M. Hassan and N. A. Peppas, "Structure and applications of poly(vinyl alcohol) hydrogels produced by conventional crosslinking or by freezing/thawing methods," *Advances in Polymer Science*, vol. 153, pp. 37–65, 2000.

[31] S. R. Stauffer and N. A. Peppast, "Poly(vinyl alcohol) hydrogels prepared by freezing-thawing cyclic processing," *Polymer*, vol. 33, no. 18, pp. 3932–3936, 1992.

[32] L. F. Gudeman and N. A. Peppas, "Preparation and characterization of pH-sensitive, interpenetrating networks of poly(vinyl alcohol) and poly(acrylic acid)," *Journal of Applied Polymer Science*, vol. 55, no. 6, pp. 919–928, 1995.

[33] R. Y. Hori and L. F. Mockros, "Indentation tests of human articular cartilage," *Journal of Biomechanics*, vol. 9, no. 4, pp. 259–268, 1976.

[34] Z. Yin, T. M. Schmid, T. K. Yasar, Y. Liu, T. J. Royston, and R. L. Magin, "Mechanical characterization of tissue-engineered cartilage using microscopic magnetic resonance elastography," *Tissue Engineering - Part C: Methods*, vol. 20, no. 8, pp. 611–619, 2014.